Development and evaluation of novel structurally simplified sialyl LewisX mimic-decorated liposomes for targeted drug delivery to E-selectin-expressing endothelial cells

(E-セレクチン発現内皮細胞への標的指向化薬物送達を目的とした新規構造単純化シアリルルイスXミミック修飾リポソームの開発と評価)

2018

CHANTARASRIVONG CHANIKARN

Contents

Preface

E-selectin is a transmembrane glycoprotein that is expressed at extremely low levels in resting endothelial cells but its expression is strongly induced via transcriptional regulation by inflammatory cytokines, such as TNF-α and IL-1β [1-3]. Induced expression of E-selectin is involved in recruitment of leukocytes in inflamed tissues as well as formation of tumor microenvironment [4-6]. Therefore, augmented expression of E-selectin in endothelial cells is an attractive target for targeted delivery of specific drugs to inflamed endothelia including tumor vasculature [7-10].

E-selectin-directed drug delivery systems have mostly utilized sialyl LewisX (sLeX), a natural ligand of E-selectin. The sLeX-decorated liposomes and nanoparticles have successfully been demonstrated to be highly accessible delivery vehicles for E-selectin targeting both in vitro and in vivo [11-16]. However, their availability is hampered by the complexity and difficulty of sLeX synthesis [17-20]. To overcome these drawbacks, the design and development of structurally simplified analogs of sLeX (so-called sLeX mimics) is promising. Therefore, this study aimed to develop novel structurally simplified sLeX analog-decorated liposomes for targeted drug delivery to E-selectin-expressing endothelial cells, that could be a potential carrier to deliver drugs to inflamed or tumor endothelium.

In chapter 1, novel sLeX mimics were designed with structural simplification to overcome drawbacks of process-intensive chemical synthesis of native sLeX. The sLeX mimics were conjugated with phospholipids to be presented on the surface of liposomes and were evaluated their targeting ability in inflammatory cytokine-treated endothelial cells. Among the sLeX mimic liposomes tested, the most potent sLeX mimic was studied further. In chapter 2, transport characteristics of the sLeX mimic liposomes were investigated in tumor spheroids with perfusable vascular network, which imitates solid tumor with blood circulation. In chapter 3, capability of the sLeX mimic liposomes in delivering drugs to E-selectin-expressing endothelial cells was investigated. In this context, anti-angiogenic drug loaded liposomes were prepared to investigate their characteristics and pharmacological effects. Details of the study will be discussed over the three chapters.

Chapter 1

Development and functional characterization of liposomes decorated with structurally simplified sLeX mimics

1-1. Introduction

E-selectin is a transmembrane glycoprotein that is expressed in endothelial cells. Its expression is extremely low in resting endothelial cells, but it is strongly induced by inflammatory cytokines such as TNF-α and IL-1β [1-3]. The physiological function of E-selectin is to support leukocyte tethering and rolling on specific locations of the endothelium and allow for further strong integrin-mediated interactions. Leukocytes recruited at the site of inflamed tissues remove pathogens and cellular debris and produce growth factors for tissue repair. Therefore, the expression of E-selectin is involved as an initial trigger in attenuating acute inflammatory injury. However, it is also known that the same mechanism occurs during the development of tumor tissues [4-6]. Cancer cells and tumor stroma produce cytokines to activate the vascular endothelium, recruit and tame innate immune cells, and form a robust immunosuppressive network called the tumor microenvironment.

Augmented expression of E-selectin in endothelial cells at inflamed or tumor tissues is an attractive option for targeted delivery of specific drugs to these tissues. As has been reviewed elsewhere [7-10], several types of E-selectin-directed drug delivery systems, *i.e.*, lipid- or polymer-based nanoparticles decorated with anti-E-selectin antibodies and small molecular ligands, have been designed and functionally characterized. Studies on immunoliposomes bearing anti-E-selectin antibodies were conducted a relatively long time ago. The first demonstration of this concept was undertaken by Bendas et al. in 1998 [21], and was later expanded by their group and other groups [22-25]. However, sialyl Lewis^X (sLeX, Neu5Acα2-3Galβ1-4(Fucα1-3)GlcNAcβ) tetrasaccharide-decorated nanoparticles have also been studied [26-29]. sLeX is a naturally occurring E-selectin ligand and is found at the terminus of N- or O-glycans and glycolipids on the surface of leukocytes and tumor cells. Use of such a small molecular ligand is beneficial due to lower immunogenicity compared with the use of immunoliposomes [30,31]. However, although sLeX-decorated liposomes and nanoparticles have successfully been demonstrated to be highly accessible delivery vehicles for E-selectin targeting both in *vitro* and in *vivo* [11-15, 32], their availability is hampered by the complexity and difficulty of sLeX synthesis. The large-scale production of sLeX is costly, requires considerable technical expertise, and involves many synthesis steps [20, 33-35]. To overcome these drawbacks, the design and development of structurally simplified analogs of sLeX (so-called sLeX mimics) is promising.

Binding between sLeX and selectins have intensively been investigated in both functional and structural studies. Systematic replacement of the functional groups of sLeX with hydrogen revealed that all three OH groups of the Fuc, the 4- and 6-OH groups of the Gal, and the COO^- group of the NeuAc are required for sLeX to bind to E- and L-selectins [36,37]. In addition, it has been reported that the GlcNAc residue does not play a crucial role in binding. Crystallographic analysis of E-selectin and sLeX cocrystals supports the results of functional studies [38-40]. The 3- and 4-OH groups of the Fuc form a network of interactions with the selectin-bound Ca^{++} ion and several amino acid residues, while the 4- and 6-OH groups of the Gal and the COO^- group of the NeuAc are responsible for further hydrogen-bond formation. Accordingly, substitution of NeuAc with a negatively charged group, such as carboxymethyl, sulfate, and phosphate groups, on the 3' position of the Gal would be the most straightforward way to simplify the structure of sLeX [41-43]. Taking into account that the GlcNAc residue is not responsible for binding, Brandley, et al [44] previously proposed and demonstrated the feasibility of fucosylated 3'-sulfo-lactose as a potent and convenient sLeX mimic. Replacement of the Gal-GlcNAc disaccharide unit with lactose (*i.e.*, Gal-Glc) removes many initial steps.

In this chapter, based on reported structure-activity studies of sLeX and its mimics [36, 44-46], novel glycolipids that are available for E-selectin-targeted drug carriers were designed and synthesized in collaboration with Drs. Kiso and Ando, Gifu University. sLeX and its mimics were conjugated with 1,2-distearoyl-*sn*-glycero-3-phosphoethanolamine-polyethyleneglycol-2000 (DSPE-PEG), taking into account that the swollen layers formed with PEG chains are required for steric protection of particulate drug carriers [47-50]. Three fucosylated lactose derivatives modified on the 3' position of the lactose unit, *i.e.*, 3'-sulfo, 3'-carboxymethyl (3'-CM), and 3'-(1-carboxy)ethyl (3'-CE), were synthesized as sLeX mimics. On the basis of previous results of sLeX mimic development [44, 51], it has been expected that fucosylated 3'-sulfo-lactose would be a suitable targeting motif because of its binding affinity to E-selectin. The 3'-CM and 3'-CE analogs were newly designed as more chemically stable analogs than the 3'-sulfo (Scheme 1). These analogs retain the position of the COO^- group of NeuAc within sLeX and are expected to engage in hydrogen-bond formation similar to sLeX. In addition, the 3'-CE analog was anticipated to provide strong interaction to E-selectin because the methyl group of the 3'-CE group limits the free rotation of the COO^- group.

The sLeX mimics-DSPE-PEG conjugates were added to prepare liposome formulations intended for E-selectin-targeted drug delivery. Uptake characteristics of the sLeX mimic liposomes were delineated in a model of e-selectin overexpressing endothelial cells. A molecular mechanism underlying the binding of sLeX mimics with E-selectin were also confirmed in molecular dynamics studies.

1-2. Materials and Methods

1-2-a. Synthesis of sLeX mimic-linked phospholipids

The targeting motifs were synthesized using an efficient, stereoselective route (Scheme 1). First, 3-aminopropyl lactoside **1** was prepared according to a previously reported procedure [52], and it was then converted into the mono-hydroxy form **2** through a four-step reaction sequence. Next, compound **2** underwent α-selective fucosylation with donor **3** with the assistance of the synergistic solvent effect of CPME-CH_2Cl_2 [53], followed by replacement of the MBn group with an acetyl group and the acid hydrolysis of the isopropylidene group at C3' and C4', producing **4**. 3'-OH selective sulfonylation, carboxymethylation and 1-carboxyethylation via tin acetal formation and subsequent full deacylation produced 3'-sulfo and 3'-carboxymethyl and 3'-(1-carboxy)ethyl trisaccharides, respectively. Finally, they were conjugated with DSPE-PEG to create sLeX mimic targeting motifs **5**, **6** and **7**, respectively.

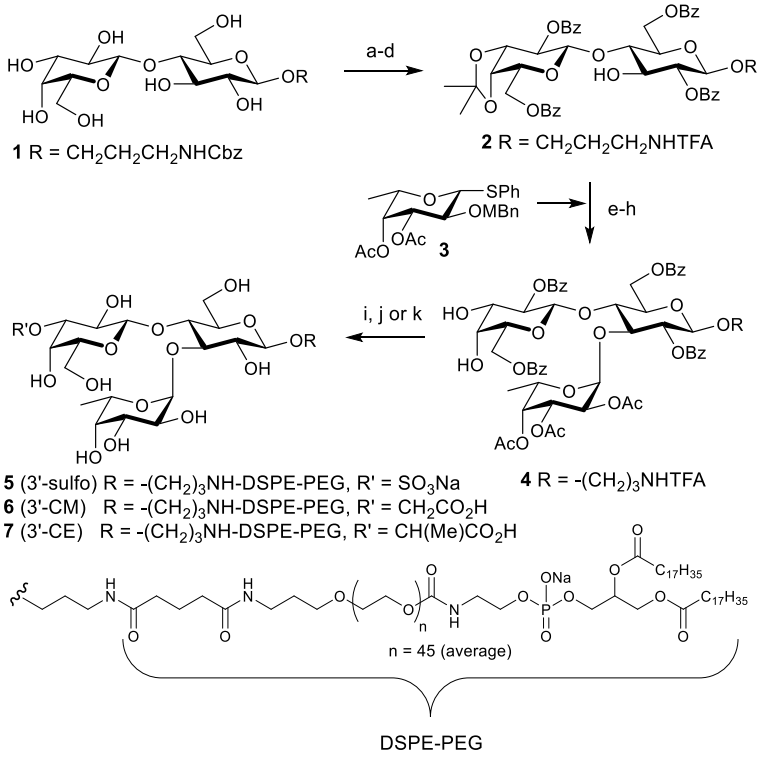

Scheme 1. Synthesis of sLeX mimic-linked phospholipids. (a) CSA/2,2-dimethoxypropane, acetone, MeCN, RT, 1 d, 63%; (b) H_2, 5% Pd/C/1,4-dioxane-H_2O (2:1), RT, 6 h; (c) TFAOMe, Et_3N/MeOH, RT, 4 h, 89% (2 steps); (d) BzCl/toluene-pyridine (4:3), 0°C, 1.5 h, 64%; (e) 3, NIS, TfOH, MS4Å/CPME-CH_2Cl_2 (1:1), -40°C, 1 d; (f) DDQ/CH_2Cl_2-H_2O (10:1), RT, 6 h; (g) Ac_2O/pyridine, RT, 2 h, 49% (3 steps); (h) 80% TFAOH aq./CH_2Cl_2, 0°C, 0.5 h, 98%; (i) i. *n*Bu_2SnO/toluene, reflux, 5 h; ii. SO_3·NMe_3/THF-DMF (4:1), RT, 15 h, 88% (2 steps); iii. 1 M NaOH aq./MeOH, RT, 21 h; iv. DSPE-PEG_{2000}-NHS /DMF-H_2O (4:1), RT, 1 h, 80% (2 steps); (j) i. *n*Bu_2SnO/toluene, reflux, 5 h; ii. ethyl bromoacetate, *n*Bu_4NI/toluene, 80°C, 5 h; iii. Ac_2O, DMAP/pyridine, RT, 6 h; iv. 1 M NaOH aq./MeOH, RT, 18 h; v. DSPE-PEG_{2000}-NHS /DMF-H_2O (4:1), RT, 1 h, 49% (5 steps); (k) i. *n*Bu_2SnO/toluene, reflux, 5 h; ii. BrCH(Me)CO_2Et, *n*Bu_4NBr/toluene, 100°C, 3 h; iii. Ac_2O, DMAP/pyridine, RT, 3 h, 44% (2 steps); iv. 1 M NaOH aq./MeOH, RT, 2 h; v. DSPE-PEG_{2000}-NHS, Me_3N/DMF-H_2O (3:1), RT, 1 h, 31% (2 steps). Cbz = benzyloxycarbonyl; TFA = trifluoroacetyl; Bz = benzoyl; MBn = *p*-methoxybenzyl; CSA = 10-comphorsulfonic acid; NIS = *N*-iodosuccinimide; CPME = cyclopentyl methyl ether; DDQ = 2,3-dichloro-5,6-dicyanobenzoquinone; DMF = *N,N*-dimethylformamide; DMAP = 4-dimethylaminopyridine; DSPE-PEG = 1,2-distearoyl-*sn*-glycero-3-phosphoethanolamine-polyethyleneglycol-2000; NHS = *N*-hydroxysuccinimidyl.

1-2-b. Preparation of liposomes

1,2-Distearoyl-sn-glycero-3-phosphocholine (DSPC) was purchased from Avanti Polar Lipids (Alabaster, AL). Cholesterol, methanol, and chloroform were purchased from Nacalai Tesque (Kyoto, Japan). DSPE-PEG-Fluorescein was prepared through the chemical reaction of DSPE-PEG-NH2 (NOF America Corporation, White Plains, NY) and Fluorescein-NHS (Thermo Fisher Scientific, Waltham, MA) following the protocol supplied by the manufacturer. DSPC (2.75 μmol/mL), cholesterol (1.95 μmol/mL), native sLeX- or sLeX mimic-linked DSPE-PEG (0.25 μmol/mL) and DSPE-PEG-Fluorescein (0.05 μmol/mL) were individually dissolved in chloroform-methanol (1:1). One milliliter of each solution was mixed in a 50-mL round-bottom flask. The solvent of the mixture was removed under reduced pressure using a rotary evaporator. The resultant lipid film was further vacuum-desiccated for at least 6 h. The lipid film was swollen using phosphate-buffered saline (PBS, Nissui Pharmaceutical, Tokyo, Japan) at room temperature for 30 min and suspended by shaking for 30 min in a water bath at 65°C. The suspension was sonicated in a bath-type sonicator (ASU-3M, AS ONE, Osaka, Japan) at 65°C for 10 min and then a tip-type sonicator (Ultrasonic generator US 300, Nissei, Tokyo, Japan) at an intensity of 200 W for 3 min. The suspension was then extruded 31 times through a 100-nm pore membrane equipped in an extruder (Avanti Mini-Extruder, Avanti Polar Lipids, Alabaster, AL) maintained at 65°C. The liposome solution was purified using a NAP-5 gel filtration column (GE Healthcare, Buckinghamshire, UK) equilibrated with PBS. After the

amount of phospholipids in the eluate was determined using a Phospholipids C-test Wako (Wako Pure Chemical Industry), the liposome concentration was adjusted to 500 nmol total lipid/mL. An aliquot of the stock solution was diluted 2.5 times with distilled water, and 750 μL of the solution was taken for measurement of the particle size and zeta potential of the liposomes in a Zetasizer Nano ZS (Malvern, Worcester, UK). Moreover, the fluorescence intensity of each liposome was determined at a total lipid concentration of 1 nmol/mL using a Fluoromax-4 spectrofluorometer (Horiba, Kyoto, Japan).

1-2-c. Cell culture

HUVECs were purchased from Kurabo Industry (Osaka, Japan) and cultured according to the protocol supplied by the manufacturer. HuMedia-EG2 (Kurabo, Osaka, Japan) was used as the culture medium. When the cells reached 70%–80% confluence, they were harvested using trypsin-EDTA, suspended in the culture medium, and plated on a dish. The rest of the cells was maintained in a flask for up to 3 generations. On day 1 after plating, the cells were pretreated with 100 ng/mL TNF-α (Life Technologies, Carlsbad, CA, USA) and 10 ng/mL IL-1β (Sigma-Aldrich, St. Louis, MO, USA) for 5 h, to induce E-selectin expression.

1-2-d. Evaluation of induction effect of TNF-α and IL-1β on E-selectin expression in HUVECs

HUVECs were harvested and suspended in the culture medium, and plated at 400,000 cells/mL in the 12-well plate on the day before experiments. TNF-α and IL-1β were added together or separately to the medium at a final concentration of 100 ng/mL and 10 ng/mL, respectively. After 5 h, cells were washed with 0.2 mL HEPES buffer (Kurabo, Osaka, Japan) and incubated with 0.2 mL of 0.0025% trypsin for 3-5 min at room temperature. The cells were then centrifuged, washed with 2 mL and resuspended with 0.3 mL of ice cold PBS. Thirty microliters of 10μg/mL anti-E-selectin antibody conjugated with FITC (Abcam, Cambridge, UK) was added and cells were incubated on ice for 30 min. The cells were washed 3 times with 2 mL and resuspended in 1 mL of ice cold PBS. Flow cytometry analysis was conducted using a FACSCanto II (BD Biosciences, San Jose, CA) with excitation and emission wavelength settings of 493 and 528 nm, respectively. Ten thousands gated cells were analyzed using fluorescence histogram with the BDFACSDiva software program.

1-2-e. Evaluation of the cellular uptake of liposomes

HUVEC were harvested, suspended in the culture medium, and plated at a density of 100,000 cells/0.5 mL in a 24-well plate on the day before experiments. Prior to uptake experiments, cytokines were added into the medium and the cells were incubated for another

5 h. At the onset of the uptake experiments, the culture medium was replaced with medium containing fluorescein-labelled liposomes (50 nmol total lipid/mL). Following incubation for the indicated time periods, the cells were washed with PBS and incubated with 0.3 mL of 0.0025% trypsin for 3–5 min at room temperature. The cells were then centrifuged and resuspended in 0.2 mL of ice-cold PBS. Flow cytometry analysis was conducted using a FACSCanto II with excitation and emission wavelength settings of 494 and 519 nm, respectively. Ten thousand gated cells were analyzed using a fluorescence histogram with the BDFACSDiva software program.

1-2-f. Confocal fluorescence microscopy analysis of the subcellular distribution of liposomes

HUVECs were harvested, suspended in the culture medium, and plated at a density of 40,000 cells/0.25 mL in an 8-well chamber slide on the day before the experiments. Prior to the experiments, cytokines were added into the medium and the cells were incubated for another 5 h. At the onset of the uptake experiments, the culture medium was replaced with medium containing fluorescein-labelled liposomes (50 nmol total lipid/mL). After incubating for 3 h, the cells were washed 3 times with PBS and fixed with 4% paraformaldehyde phosphate buffer solution (Nacalai Tesque, Kyoto, Japan). Fifteen minutes later, the cells were washed with PBS, mounted with Vectashield mounting medium containing DAPI (Vector laboratories Inc, Burlingame, CA), and observed using a confocal microscope (Nikon A1RMP/Ti-E/PFS, Nikon Instruments Inc., Melville, NY) equipped with NIS-elements AR 4.13.00 software. The excitation wavelength was set at 488.5 nm and 404 nm, and the emission wavelengths were scanned in the range of 500-550 nm and 425-475 nm for fluorescence and DAPI, respectively.

1-2-g. Evaluation of specific process of cellular uptake/association of liposomes in HUVECs

For cellular specific process of uptake study, HUVECs were harvested, and suspended in the culture medium, and plated at a density of 100,000 cells/0.5 mL in a 24-well plate on the day before the experiments. After 5h of cytokines treatment, the culture medium was replaced with that containing fluorescein-labeled liposomes (50 nmol total lipid/mL). After incubating for 3 h, the cells were prepared and analysed using flow cytometry with the same method as previous uptake study.

For specific process of cellular association study, HUVECs were harvested, suspended in the culture medium, and plated at a density of 40,000 cells/0.25 mL in a 48-well plate on the day before the experiments. Following a 5-h cytokine treatment, the culture medium was

replaced with an equal volume of Hank's buffered salt solution (HBSS) (Nissui Pharmaceutical, Tokyo, Japan) containing one of the anti-selectin antibodies (Abcam, Cambridge, UK) at a concentration of 10 μg/mL, and the cells were then incubated for 30 min on ice. Twenty-five microliters of 500 nmol total lipid/mL liposome solution was added at the onset of the cellular association study. Fifteen minutes later, the cells were washed twice with 0.3 mL of HBSS supplemented with 10% fetal bovine serum (FBS) and once with 0.3 mL of HBSS and then lysed with 0.1 mL of an aqueous lysis buffer composed of 0.05% Triton X-100, 0.075% EDTA, and 1.21% Tris for 15 min on a shaker. The lysates were transferred to a 96-well plate, and their fluorescence intensity was determined using an ARVO MX microplate fluorometer (Perkin Elmer, Waltham, MA) with excitation-emission wavelengths set at 485 and 535 nm, respectively. The protein concentration in 20-μL aliquots of the lysate was measured using the Protein Quantification Kit-Wide Range (Dojindo Molecular Technologies, Rockville, MD). In addition, the inhibitory effects of anti-selectin antibodies were statistically evaluated using a one-way analysis of variance with Dunnett's post hoc test.

1-2-h. Molecular dynamics simulation

The structure of the sLeX-E-selectin cocrystal (PDB: 4CSY) [40] was used as a template to investigate the molecular binding of sLeX mimics with E-selectin. A molecular dynamics (MD) calculation of the solvated protein-ligand complex was performed using the GROMACS 5.0.4 package [54]. The AMBER-ff99SB force field [55] and the AMBER-GAFF [56]/AM1-BCC [57] were assigned for E-selectin and ligand molecules, respectively. Each complex structure was neutralized and placed in a TIP3P [58] water box, with a margin of 10 Å between the protein and the boundaries of the periodic box. The particle mesh Ewald method with a cut-off of 8 Å was used to calculate long-range electrostatic interactions. MD simulations of 100 ps for the system relaxation under constant NVT conditions at 300 K and 400 ps for water molecule density equilibration under constant NPT conditions at 1 bar and 300 K were performed before data collection. Subsequently, an MD simulation of 2 ns was performed under constant NVT conditions at 300 K, and the complex structures were extracted in the 201 snapshots taken every 10 ps. This MD simulation scheme was replicated three times, and the analyses for hydrogen-bond formations and distributions of dihedral angles were performed in a total of 603 snapshots.

1-3. Results and Discussion

1-3-a. Synthesis of sLeX mimic-linked phospholipids

Novel glycolipids bearing sLeX mimics were designed and synthesized (Scheme1). The common intermediate 4 was synthesized in 18 steps from the starting materials (Lac and Fuc) and target compounds 5, 6, 7 were synthesized in 3 or 4 steps from 4 (total 21 or 22 steps). This synthetic route is shorter than that of the glycolipid conjugated with native sLeX tetrasaccharide (31 steps from GlcNH2, Gal, Fuc, and NeuAc) [59]. In addition, the number of glycosidation reactions, which require high expertise and laborious purification of the reaction product, were reduced to 2 times in the synthetic route, compared to that of sLeX tetrasaccharide (4 times). Therefore, the large-scale synthesis of the mimics would be possible by the synthetic route.

1-3-b. Physicochemical characteristics of native and mimic sLeX liposomes

Table 1 summarizes the particle size and zeta potential of the prepared liposomes. The average diameter was similar in all the liposomes, ranging from 96.4 to 106.4 nm. Their polydispersity indices were no more than 0.19, indicating that liposomes with a uniform size distribution were obtained by employing an extrusion method following the hydration-sonication method. Whereas the PEG liposome was nearly neutral with a zeta potential of −6.92 ± 1.23 mV, all liposomes bearing the native or mimic sLeX residues were highly negative with regard to surface charge, but the negative charges associated with native or mimic sLeX were not significantly different. The fluorescence intensities of all prepared liposomes were comparable but, to be more precise, were employed for normalization of cellular uptake.

Table 1. Physicochemical characteristics of native and mimic sLeX liposomes

Liposome[a)]	Average diameter (nm)	PDI[b)]	Zeta potential (mV)
PEG	102.53 ± 0.46	0.16	–6.92 ± 1.23
Native sLeX-PEG	98.45 ± 1.01	0.16	–24.5 ± 1.1
3'-sulfo sLeX mimic-PEG	106.37 ± 1.46	0.19	–23.97 ± 0.85
3'-CM sLeX mimic-PEG	96.35 ± 0.51	0.17	–23.03 ± 1.7
3'-CE sLeX mimic-PEG	102.33 ± 0.71	0.11	–24.70 ± 1.1

Results of diameter and zeta potential are expressed as mean ± standard deviation (SD) of three samples.

a) *PEG, polyethylene glycol; 3'-CM, 3'-carboxymethyl; 3'-CE, 3'-(1-carboxy)ethyl.*

b) PDI, polydispersity index.

1-3-c. Induction effect of TNF-α and IL-1β on E-selectin expression in HUVECs

Cytokine-stimulated HUVECs have often been used as a model of E-selectin-expressing inflammatory endothelium [60-64]. This study was done to confirm effect of cytokines on E-selectin expression of HUVECs. **Figure 1** shows that treatment of HUVECs with TNF-α or IL-1β increased the expression of E-selectin on their surface by 6.6 and 7.5 times, respectively, whereas combined treatment of both of the cytokines resulted in additive induction of expression of the E-selectin 16.9 times. This result indicated that dual pretreatment with TNF-α and IL-1β provided greater E-selectin induction than pretreatment with single cytokines. Indeed, the binding of a fluorescein-labeled anti-E-selectin antibody to HUVECs treated with dual cytokines was more than twice that of HUVECs treated with either TNF-α or IL-1β alone. Therefore, HUVECs pretreated with both TNF-α and IL-1β are best suited for this experiment.

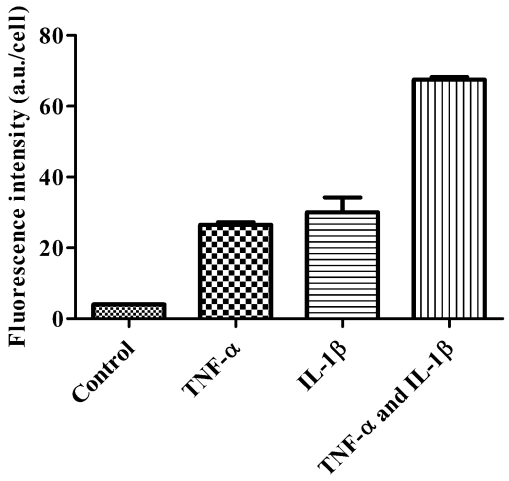

Figure 1. Effect of TNF-α and IL-1β on the expression of E-selectin on the surfaces on HUVECs. Results are expressed as mean + SD of three samples.

1-3-d. Uptake in cytokine-treated HUVECs

Figure 2A shows the time course of the uptake of native and mimic sLeX liposomes in proinflammatory cytokine-treated HUVECs. The cellular uptake of all tested liposomes increased linearly over 4 h. The uptake rate calculated from the slope was highest with the 3'-CE sLeX mimic liposomes (105.2-fold higher than that of the PEG liposome), followed by the 3'-sulfo sLeX mimic (90.1-fold), native sLeX (85.1-fold), and 3'-CM sLeX mimic liposomes (25.5-fold). Hereafter, the cellular uptake of the liposomes was evaluated at 3 h.

Figure 2B shows the concentration dependence of the liposome uptake. The uptake of native and mimic sLeX liposomes obeyed nonlinear kinetics within the concentration range tested (0.025–0.2 μmol total lipid/mL). The Eadie–Hofstee plot analysis indicated that the Michaelis–Menten constants (Km) were 0.011, 0.020, 0.025, and 0.057 μmol total lipid/mL for the 3'-CE sLeX mimic, native sLeX, 3'-sulfo sLeX mimic, and 3'-CM sLeX mimic liposomes,

respectively (**Figure 3**). The order of the affinity-related constant values corresponded to that of the uptake rate. The Km values for each type of liposome presumed that all of the ligand residues, i.e., 5 mol%, were available for specific binding. The resulting Km values are not strictly accurate because this approach does not consider what percentage of these residues are directed to the liposome surface, but it allows for a relative comparison in affinity among the liposomes. Ohmoto et al. [45] and Wada et al. [65] have investigated the binding of the 3'-sulfo sLeX mimic and native sLeX to selectin-IgG chimeras in enzyme-linked immunosorbent assay (ELISA) inhibition assays. The half maximal inhibitory concentration (IC50) values for the reported analogs [45, 65] were in the same concentration range as the Km values obtained in the current study. However, these previous studies [45, 65] have indicated that the 3'-sulfo sLeX mimic has slightly less potency than the native sLeX in binding to E-selectin, whereas our present results indicate that both are almost comparable in terms of Km. This inconsistency may be due to differences in experimental conditions: we used liposome-conjugated sLeX mimics instead of free sLeX mimics and a cell-based but not a cell-free assay.

Results from above indicating that the highest uptake was exhibited by the 3'-CE sLeX mimic liposome, whereas the 3'-CM sLeX mimic liposome had the lowest activity. Interestingly, the substitution of a proton in the carboxymethylene with a methyl group led to totally different outcomes in terms of the uptake of these 2 carboxyl-type sLeX mimic-decorated liposomes, in other words, substitution of methyl group in the carboxymethylene greatly improved the cellular uptake in E-selectin-overexpressing HUVECs.

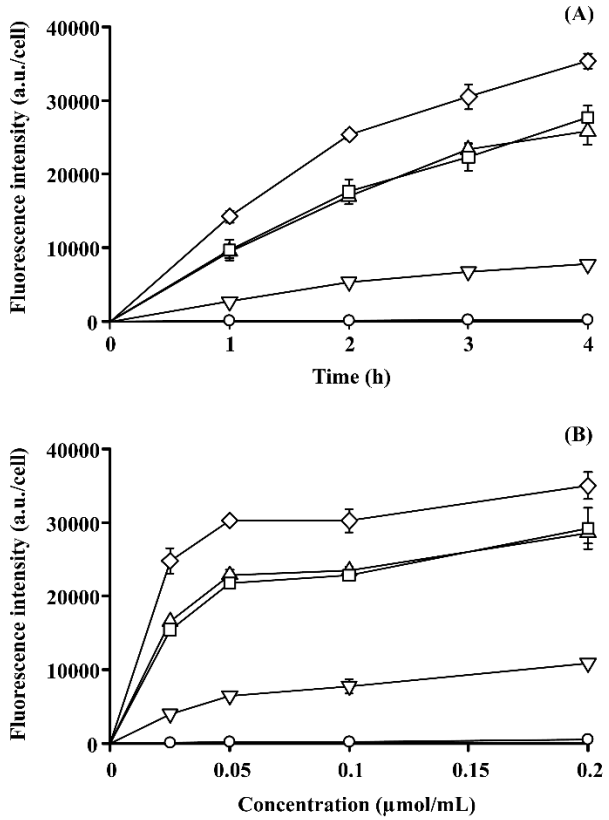

Figure 2. Time-course analyses (A) and concentration dependence (B) of the uptake of fluorescein-labeled liposomes in HUVECs treated with TNF-α and IL-1β for 5 h. Symbols: ○, PEG liposome; △, native sLeX liposome; □, 3'-sulfo sLeX mimic liposome; ▽, 3'-CM sLeX mimic liposome; ◇, 3'-CE sLeX mimic liposome. Results are expressed as mean ± SD of three samples.

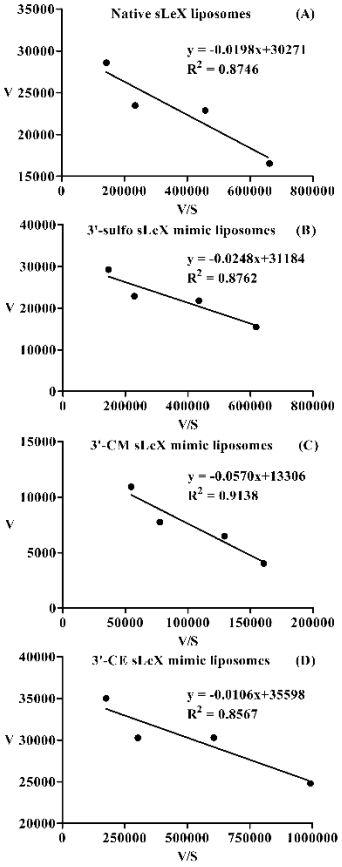

Figure 3. Eadie–Hofstee diagrams of the uptake of (A) native sLeX, (B) 3'-sulfo sLeX mimic, (C) 3'-CM sLeX mimic, and (D) 3'-CE sLeX mimic liposomes in HUVECs pretreated with 100 ng/mL TNF-α and 10 ng/mL IL-1β for 5 h. The ordinate and abscissa represent the uptake rate (v) and the uptake rate divided by liposome concentration (v/s), respectively. The regressed equation, together with its regression coefficient, is shown in each panel, where

$$v = -K_m \cdot \frac{v}{s} + V_{max}$$

To confirm the cellular internalization of the liposomes, confocal fluorescence microscopy was employed. **Figure 4** shows the subcellular distribution of fluorescence signals in proinflammatory cytokine-treated HUVECs at 3 h following the application of each type of liposome. In contrast to PEG liposomes, high fluorescence signals were detected throughout the entire cell interior when native sLeX or 3'-CE sLeX mimic liposomes were applied. In

addition, bright granular spots of fluorescence were found in the subcellular compartment, suggesting endocytic internalization of sLeX liposomes. Although fluorescent intensity of 3'-CE sLeX mimic liposomes was significantly greater than that of native sLeX liposomes, profiles of subcellular fluorescence distribution were similar. Thus, structural simplification of the ligand was unlikely to functionally alter the cellular internalization process of sLeX liposomes.

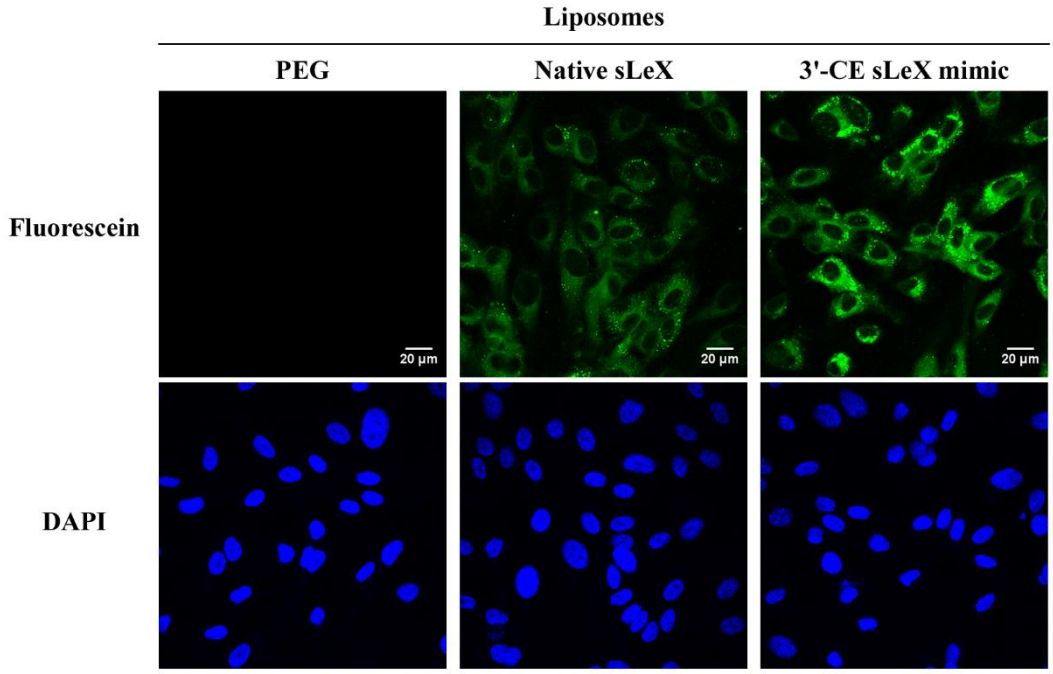

Figure 4. Confocal fluorescence microscopy of subcellular distribution of PEG, native sLeX, and 3'-CE sLeX mimic liposomes in HUVECs treated with TNF-α and IL-1β. The images were taken at 3 h following application of the liposomes to the cells. The liposomes were labeled with DSPE-PEG-Fluorescein (green color). The cells were stained with DAPI (blue) following fixation with 4% paraformaldehyde. The bar represents 20 μm.

1-3-e. Specific process of cellular uptake/association of liposomes in HUVECs

Figure 5 shows that cellular uptake of native and mimic sLeX liposomes in cytokine-treated HUVECs was 2 orders of magnitude higher than that in nontreated HUVECs, whereas the uptake of PEG liposomes was similar in both cytokine-treated and nontreated cells. Such a big difference is possibly due to augmented expression of E-selectin by treatment with TNF-α and IL-1β. The cellular uptake of 3'-CE sLeX mimic liposomes was also compared in between different ligand densities. The uptake of 3'-CE sLeX-mimic liposome was only 1.2 times different in between the two concentrations of 2.5% and 5%, suggesting that the ligand density of 5% would be high enough.

To confirm whether the increased uptake is due to E-selectin mediated processes, the effect of specific antibodies on the cellular association of the liposomes was investigated. **Figure 6** shows the cellular association of native and mimic sLeX liposomes in the presence and absence of specific antibodies against E-selectin, P-selectin, or L-selectin (10 μg/mL). The anti-E-selectin antibody inhibited the cellular association of native sLeX, 3'-sulfo sLeX mimic, and 3'-CE sLeX mimic liposomes by 70%, 72.7%, and 91.7%, respectively, whereas significant inhibition did not occur for the 3'-CM sLeX mimic liposome. In contrast, neither the anti-P-selectin nor anti-L-selectin antibodies affected the cellular association of any of the liposomes. Therefore, the uptake of native and mimic sLeX liposomes was considered to be mediated mostly by E-selectin, the expression of which was upregulated by pretreatment with TNF-α and IL-1β. An anti-P-selectin antibody did not affect the association of any of the liposomes tested, despite previous reports that sLeX is a P-selectin ligand [66-68]. This is likely because of the low expression of P-selectin in HUVECs regardless of treatment with inflammatory cytokines such TNF-α and IL-1β [69, 70].

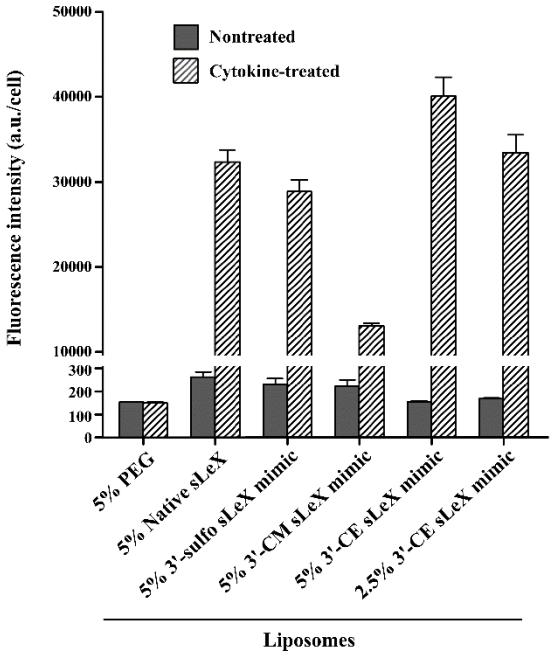

Figure 5. Uptake of fluorescein-labeled liposomes for 3 h in HUVECs treated or nontreated with TNF-α and IL-1β. Results are expressed as mean + SD of three samples.

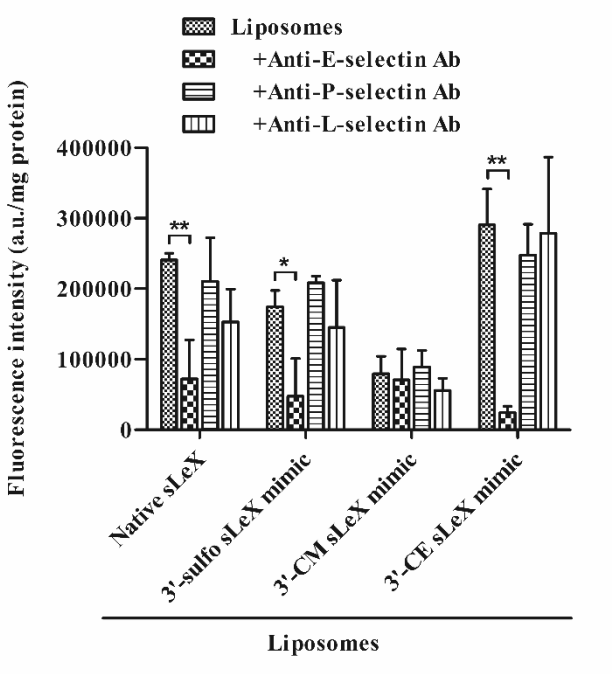

Figure 6. Inhibition by anti-selectin antibodies of the association of fluorescein-labeled native and mimic sLeX liposomes with HUVECs treated with TNF-α and IL-1β. Results are expressed as mean + SD of three samples. *P<0.05. **P<0.01.

1-3-f. Molecular dynamics simulation of the interaction of native and mimic sLeX with E-selectin

Two new sLeX mimics (i.e., 3'-CM and 3'-CE sLeX mimics) were designed and synthesized in this study, which have been modified from previously reported carboxyl-type mimics [71, 72] by taking into consideration the ease and efficiency of their synthesis. Interestingly, the substitution of a proton in the carboxymethylene with a methyl group led to totally different outcomes in terms of the uptake of carboxyl-type sLeX mimic-decorated liposomes in E-selectin-overexpressing HUVECs (**Figure 1**). To gain insight into the mechanism, MD simulation studies were conducted.

Differences in binding free energy between the liposomes estimated from experimental Km values were at most ~1 kcal/mol, which is considered to be too small for quantitative evaluation by MD simulation. Therefore, qualitative evaluations on binding modes to E-selectin, i.e., hydrogen-bond formation and distribution of dihedral angles were conducted. Even though, many interactions occur in the binding of sLeX to E-selectin, including calcium-mediated binding of the 2- and 3-hydroxyl groups of fucose, hydrogen bonding of hydroxyl groups of fucose and galactose to Glu80 or Tyr94, and hydrogen bonding between the carboxyl group of NeuAc and Arg97 [37, 73], it was sufficient to pay attention to interactions between the 3'-position group of galactose and the amino acid residues of E-selectin as a result of the structures of native sLeX and the 3'-CM and 3'-CE sLeX mimics.

One identified mode of interaction was the formation of hydrogen bonds between the 3'-position group of the sLeX mimics and amino acid residues of E-selectin, for which the phenolic oxygen of Tyr48 (Tyr48-Oη) and the guanidine nitrogens of Arg97 (Arg97-Nε, Arg97-Nη) were responsible (**Figure 7**). Taking the cut-off for hydrogen-bond distance as 3.2 Å, the probability of each intermolecular hydrogen-bond formation was calculated from a total of 603 snapshots during MD simulations (**Table 2**). The 3'-CM sLeX mimic can form a hydrogen bond only with Tyr48-Oη, with much lower probability compared with the native sLeX and 3'-CE sLeX mimic. In contrast, the 3'-CE sLeX mimic can form hydrogen bonds simultaneously with all three possible atoms. This is in agreement with the higher uptake of the 3'-CE sLeX mimic liposome in cytokine-stimulated HUVECs compared with the other liposomes.

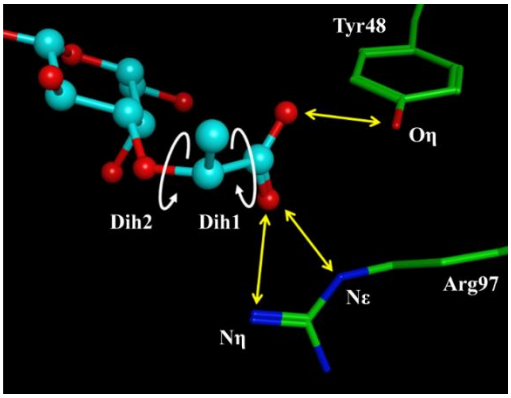

Figure 7. A snapshot of the molecular interaction of the 3'-position group of the 3'-CE sLeX mimic with the amino acid residues of E-selectin.

Table 2. Probability of each intermolecular hydrogen-bond formation between the 3'-position group of sLeX mimics and the amino acid residues of E-selectin

	Hydrogen-bond formation probability (%)		
	Tyr48-Oη	Arg97-Nε	Arg97-Nη
Native sLeX	93.7	61.9	29.4
3'-sulfo sLeX mimic	52.7	49.8	10.8
3'-CM sLeX mimic	57.5	20.4	11.3
3'-CE sLeX mimic	84.9	77.6	81.8

In addition, the probability density distribution for two dihedral angles, i.e., the dihedral angles of O(carboxylate)-C-C-O(ether) (Dih1) and of C(carboxylate)-C-O(ether)-C(galactose) (Dih2), was calculated to evaluate the rotational degrees of freedom of the 3'-position functional groups. The Dih1 for native sLeX provided a single-peak distribution around –70°, indicating highly restricted rotation of the carboxylate group. The 3'-CE sLeX mimic mostly kept the carboxylate plane at the same angle as that of native sLeX, although the carboxylate plane could sometimes be inverted (indicated by a small peak at 80°). However, the distribution of the Dih1 for the 3'-CM sLeX mimic was much broader, implying that its carboxylate group is more freely rotatable. With regard to the Dih2, no remarkable peaks were observed with any of the ligands (**Figure 8**). When the 3'-CE sLeX mimic has the primary conformation, the terminally branched methyl group is oriented and faces the bulk hydrophilic solution in spite of its hydrophobic nature (**Figure 9**). Since this state is entropically unfavorable, the 3'-CE sLeX mimic molecule might be pushed toward the binding pocket of E-selectin by a hydrophobic effect. In contrast, the carboxyl group of native sLeX had a fixed direction because of the bulky sugar group. Although the conformation is stable in native sLeX, such an entropic effect as that seen in the 3'-CE sLeX mimic would not exist because its

sugar group is hydrophilic. Therefore, differences in the interaction of the ligands with bulk water might explain the stronger binding of the 3'-CE sLeX mimic to E-selectin.

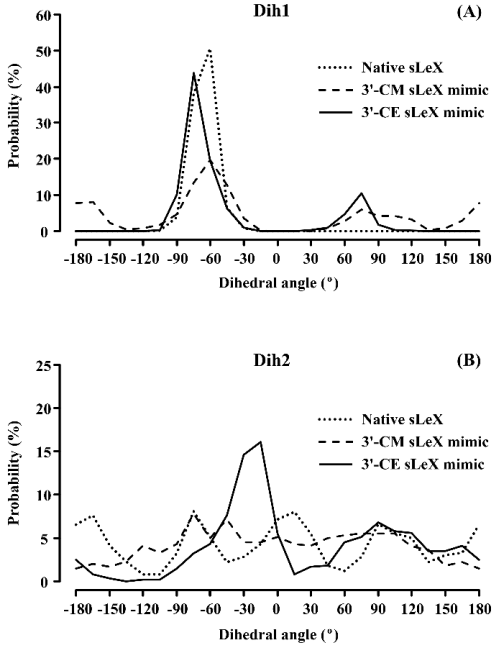

Figure 8. Density distribution for the dihedral angles of O(carboxylate)-C-C-O(ether), Dih1 (A) and of C(carboxylate)-C-O(ether)-C(galactose), Dih2 (B) in the 3'-position functional group of native sLeX (dotted line), 3'-CM sLeX mimic (dashed line), and 3'-CE sLeX mimic (solid line) complexed with E-selectin. The distribution profiles were obtained from a total of 603 snapshots (every 10 ps for 2 ns, 3 runs) during MD simulation.

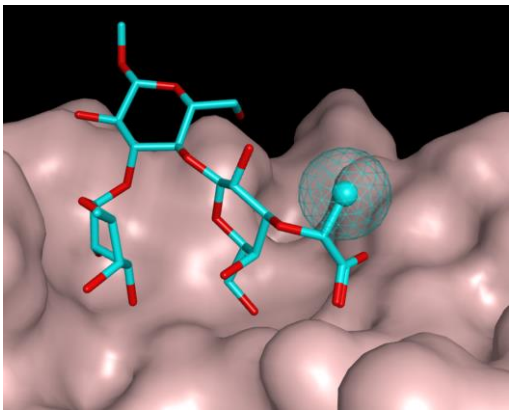

Figure 9. Binding position of the 3'-CE sLeX mimic. The terminally branched methyl group is shown in a mesh sphere.

1-4. Conclusion

Novel sLeX mimics were successfully developed with a less complicated synthesis and improved activity. In a liposome delivery system, the 3'-CE sLeX mimic liposome showed the highest uptake in E-selectin-overexpressing HUVECs. MD simulation studies demonstrated that the 3'-CE sLeX mimic is more strongly bound to E-selectin than native sLeX, because of the higher probability of hydrogen-bond formation. Therefore, the 3'-CE sLeX mimic liposome has a greater potential for targeted drug delivery to the endothelium of inflamed tissues and tumor tissues.

Chapter 2

Transport characteristics of 3’-(1-carboxy)ethyl sialyl LewisX mimic liposomes in tumor spheroids with a perfusable vascular network

2-1. Introduction

Tumor vasculature targeting is one of the promising approaches in cancer therapy. Solid tumors require angiogenesis to secure the supply of oxygen and nutrients for survival. Inhibition of angiogenesis shut out the supply of these essential substances, leading to suppression of tumor growth. Thereby, a potential advantage of this approach is to be applied to any solid tumors. Moreover, extravasation of drug delivery carriers through the vessels is not required, providing higher opportunity to interact with target cells as compared to direct cancer cell targeting [74-76].

In vivo distribution of drug delivery systems following intravenous injection is routinely evaluated, but provides limited information on the disposition behaviors in tumor tissues. To gain the mechanistic aspect, several tumor vasculature models have been developed, including dorsal chamber models [77-79] and tissue-isolated perfused tumor [80]. Although dorsal chamber models were used, a surgery step or membrane irritation in the chamber area may interfere vascular response or angiogenesis results [81]. In addition, preparation of in vivo models is time consuming and prone to variability [82].

A spheroid or multicellular aggregate is a three-dimensional cell model that mimics in vivo cellular functions [83, 84]. Cells in a spheroid are exposed to different states depending on their positions and interact or communicate mutually [85]. The 3D environment influences cellular response to foreign substances or drugs in a complex way similar to the body system. Therefore, spheroids have been used widely for biomedical research including drug delivery [86, 87].

Recent progress on spheroid culture models includes a spheroid with perfusable vascular networks in microfluidic device. It resembles in vivo situations such as exchange of substances between luminal vessels and spheroidal tissues. Spheroid with perfusable vascular networks was prepared by getting a co-culture spheroid of human umbilical vein endothelial cells (HUVECs) and normal human lung fibroblasts (nhLFs) jointed spontaneously with sprouting HUVECs from microchannels in a microfluidic device [88-91]. The nhLFs release growth factors necessary for angiogenesis to support the vessel formation from HUVECs in both spheroid and microchannels, just like as fibroblasts do in tumor tissues in vivo [92]. Along the culture time, angiogenic sprouts were developed from spheroids and both sides of microchannels and connected, eventually forming continuous vascular networks.

In this chapter, spheroids with cancer cells and perfusable vascular networks were developed to evaluate disposition behaviors of sLeX mimic-decorated liposomes. Nashimoto Y, et al. (2018) have previously found that MCF-7, a human breast cancer cell line, forms spheroids with HUVECs and nhLFs without disturbing development of perfusable vascular networks [93]. Here, E-selectin expression were preliminarily evaluated in tumor spheroids composed of HUVECs, nhLFs, and MCF-7. The tumor spheroid with perfusable vascular network was prepared, with expression of E-selectin induced by cytokines. After the perfusability of the system was confirmed, dynamic disposition behavior of 3'-CE sLeX mimic liposomes, the most potent in E-selectin-mediated delivery in chapter 1, were investigated.

2-2. Materials and Methods

2-2-a. Preparation of fluorescent-labelled liposomes

Dy590-labelled liposomes, 3'-CE sLeX mimic liposomes and control pegylated liposomes, were prepared according to the hydration method [94], reported in chapter 1. Briefly, DSPC, cholesterol, 3'-CE sLeX mimic-linked DSPE-PEG, and DSPE-PEG-Dy590 were mixed in chloroform-methanol (1:1) at the molar ratio of 55:39:5:1 and then dried under reduced pressure using a rotary evaporator and vacuum desiccator. The lipid film was swollen and suspended in PBS at 65°C. The suspension was sonicated in a bath-type sonicator at 65°C for 10 min and with a tip-type sonicator for 3 min, and then extruded through a 100 nm pore membrane equipped in an extruder maintained at 65°C. The liposome solution was purified using a PD-10 gel filtration column. Lipid concentration was determined using a Phospholipids C-test Wako (Wako Pure Chemicals, Osaka, Japan) and particle size and zeta potential were measured using a Zetasizer Nano ZS (Malvern, Worcester, UK). Before perfusion experiment, the liposomes were diluted with EGM-2 medium (Lonza, Basel, Switzerland) to yield a concentration of 0.025 μmol/mL. Possible aggregates were removed using 0.45 μm Cosmonice filter W (Nacalai Tesque, Kyoto, Japan) and fluorescent intensity of each liposomes was determined using a spectrofluorometer (Horiba, Kyoto, Japan).

2-2-b. Preparation of tumor spheroid with perfusable vascular network

- Spheroid preparation

Green fluorescent protein expressing HUVECs, GFP-HUVECs (Angio-proteome, Boston, MA), were cultured in EGM-2 medium (Lonza, Basel, Switzerland). Normal human lung

fibroblasts, nhLF, were purchased and cultured in FGM-2 medium from Lonza (Basel, Switzerland). MCF-7 cancer cells were obtained from Riken BRC cell bank (Ibaraki, Japan) and cultured in MEM medium (Nacalai Tesque, Kyoto, Japan) supplemented with 10% FBS and 1mM sodium pyruvate. When the cells reached 70–80% confluence in a 100-mm dish, the cells were harvested using 0.05% trypsin-EDTA and separately suspended in EGM-2 medium. GFP-HUVECs, nhLF, and MCF-7 were mixed to final cell concentrations at 25,000 cells/mL, 75,000 cells/mL, and 25,000 cells/mL, respectively. Two hundred microliters of mixed cell suspension were gently added to each well of 96-well plate with ultra-low attachment surface (Sumitomo Bakelite, Tokyo, Japan), and then the plate was incubated at 37 °C and 5% CO_2 for 2 days.

- Spheroid loading

Microfluidic devices [91] were sterilized under UV light in biosafety cabinet for 1-2 h before spheroid loading. All the steps hereafter was performed on ice in order to prevent gelation of collagen and fibrin. Collagen (Corning, Bedford, MA) was neutralized in PBS with 0.064% NaOH at a final concentration of 3.0 mg/mL. Fibrinogen and thrombin were purchased from Sigma-Aldrich (St. Louis, MO) and dissolved in PBS at a final concentration of 2.80 mg/mL and 50 U/mL, respectively. The neutralized collagen (64 µL), fibrinogen solution (857.6 µL), and aprotinin (28.8 µL, Sigma-Aldrich, St. Louis, MO) were mixed in 1.5 mL tube and labelled as master mix solution (MS). Ten-µL and 200-µL pipette tips were trimmed until their caliber sizes were slightly larger than the diameter of holes of the microfluidic device. A 35-mm petri dish was placed on ice and 99 µL MS was added on the dish to form a droplet. One spheroid grown in the ultra-low attachment 96-well plate was pipetted using a trimmed 200-µL pipette tip and sedimented to the tip of the pipette tip. The spheroid was transferred with a minimal volume into the MS droplet with keeping the tip of the pipette tip contacted on the surface of the droplet meniscus. Immediately after 1 µL of 50 U/mL thrombin was added, the suspension with a single spheroid was mixed gently by pipetting with a trimmed 200-µL tip. The spheroid was pipetted with a pipette set to deliver 7 µL with trimmed 10-µL tip and slowly injected into the middle hole of the device. After uniform distribution of the injected solution throughout the central compartment of the device without leakage to microchannels was confirmed, the device was incubated at 37 °C for 15 min for complete gelation of fibrin. Microchannels along the both sides of the central compartment were then filled with 60-70 µL EGM-2 medium for each. The device was placed in a 100-mm dish with a wet tissue paper

to prevent media evaporation and incubated at 37 °C, 5% CO_2 for 24 h to remove small bubbles in the device.

- HUVECs loading

GFP-HUVECs were harvested using 0.05% trypsin-EDTA, resuspended in EGM-2 medium at a density of 5,000,000 cells/mL, and then injected into one microchannel of the device using a pipette with trimmed 200-µL tip. The device was tilt vertically with the cells-loaded microchannel upside , placed in an incubator at 37 °C for 30 min, so that the cells can be sedimented to microslits and attached to allow cell adhesion to the fibrin gel through microslits. After confirmation of the cell attachment, GFP-HUVECs were loaded into the other microchannel and allowed to adhere to the fibrin gel in the same manner. The medium was changed every other day for 7 days. Vascular network formation of GFP-HUVECs was investigated using fluorescence microscope, Olympus IX73 equipped with AdvanCam-E3Rs camera and AdvanView software.

2-2-c. E-selectin expression

E-selectin expression in monolayer cells and spheroids was quantified by quantitative reverse transcriptase polymerase chain reaction (qRT-PCR) technique. In case of 2D culture, cells were cultured until being sub-confluent in 35-mm dish, treated with 350 µL lysis buffer mixed with 3.5 µL β-mercaptoethanoland harvested by a cell scrapper. In case of 3D culture, 10-15 spheroids were collected from each well and treated with the same β-mercaptoethanol-containing lysis buffer. Both cell and spheroid suspensions were repeatedly sucked up and down with a 22G needle syringe 10 times, transferred to with NucleoSpin filter device (Machery-Nagel, Duren, Germany), and filtered under centrifugation at 11,000g for 1 min. The filtrate was stored in -80 °C until the next step was done. Reverse transcription and qPCR preparation were performed using PrimeScript RT Master Mix (Perfect real time) and qPCR reagent TB Green Premix Ex Taq II (Takara Bio, Kusatsu, Shiga) following the manufacturer's protocol. Primer sequences were designed as follows: E-Selectin_For: 5'-GAAGGATGGACGCTCAATGG-3' and E-Selectin_Rev: 5'-TGGACTCAGTGGGAGCTTCAC-3', CD31_For: 5'-AAACCACTGCAGAGTACCAGG-3' and CD31_Rev: 5'-GCCTCTTTCTTGTCCAGTGTC-3', β-actin_For: 5'- CCAACCGCGAGAAGATGA-3' and β-actin_Rev: 5'- CCAGAGGCGTACAGGGATAG-3'. The PCR reactions were carried out in QuantStudio 5 Real-Time PCR system (Applied Biosystems, Foster City, CA) under the following conditions: 95 °C for 30 sec, followed by 50 cycles of 95 °C for 5 sec and 60 °C for 30 s. Relative gene expression

levels were determined by analyzing the changes in SYBR green fluorescence during qRT-PCR using the ΔΔCt method. Melting curve profiles were evaluated at the end of each reaction to confirm amplification of specific transcripts. Messenger RNA level of E-selectin was normalized with that of β-actin or CD31 used as an internal control.

2-2-d. Fluid perfusion and imaging

To investigate disposition behavior of liposomes in tumor spheroid with perfusable vascular network, real-time imaging of fluorescent-labelled liposomes was performed under fluorescence microscope. Prior to the experiment, medium was replaced with fresh culture medium supplemented with 100 ng/mL TNF-α (Life Technologies, Carlsbad, CA) and 10 ng/mL IL-1β (Sigma-Aldrich, St. Louis, MO) to stimulate E-selectin expression of GFP-HUVECs in the vascular network. After 4h, medium was removed and the device was set under fluorescence microscope. Real-time imaging was started before the liposomes were introduced to a hole of one side-channel and continued for 10 min. The fluid flow was driven by liquid level difference between two side-channels.

2-3. Results and Discussion

2-3-a. Physicochemical characteristics of fluorescent-labelled liposomes

Table 1 summarizes characteristics of liposomes used for this study. The fluorescent-labelled liposomes prepared were comparable in size and fluorescent intensity. The average diameter was approximately 90 nm for both PEG-liposomes and 3'-CE sLeX mimic liposomes. Their small polydispersity indices indicate that both liposomes have a uniform size with narrow distribution. The 3'-CE sLeX mimic liposome was highly negative with a zeta potential of −21.3 mV and PEG-liposomes was slightly negative. They were comparable to liposomes prepared in chapter 1.

Table 1. Characteristics of liposomes used in this study

Liposomes	Average diameter (nm)	Polydispersity index	Zeta potential (mV)	Fluorescent intensity (RFU)
Dy590-labelled PEG	96.70 ± 1.05	0.09	-5.65 ± 0.99	369
Dy590-labelled 3'-CE sLeX mimic	88.01 ± 0.39	0.12	-21.30 ± 1.56	385

Results of diameter and zeta potential are expressed as mean ± SD of three samples.

2-3-b. Development of tumor spheroid with perfusable vascular network

Development of tumor spheroid with perfusable vascular network was investigated using GFP-HUVEC. **Figure 1A** shows development of vessels, vascular network formed by HUVECs in tumor spheroid and in microchannels of the microfluidic device. In the first few days, vessel-like structure in tumor spheroid and small angiogenic sprouts from open microchannels were formed. With time, angiogenic sprouts became more abundant and branched, but elongated to attract each other between different ends. On day 7, continuous vascular network of HUVECs was completely formed. The vascular vessels were varied and uncontrolled in size, but provided the ability of perfusion. Uneven size of vessels is likely similar to that of blood vessels in vivo tumor tissues [95, 96]. After repeated trials and failures of the preparation, it was found that the tumor spheroid must be placed in the same planar as HUVECs sprouting from the microchannel sides. Otherwise angiogenic sprouts could not make connections tightly, resulting in incapability of perfusing the network. **Figure 1B** shows a typical failure of preparations in which, when injected into the central well of the device, the spheroid did not sediment to the bottom before starting gel formation of fibrin.

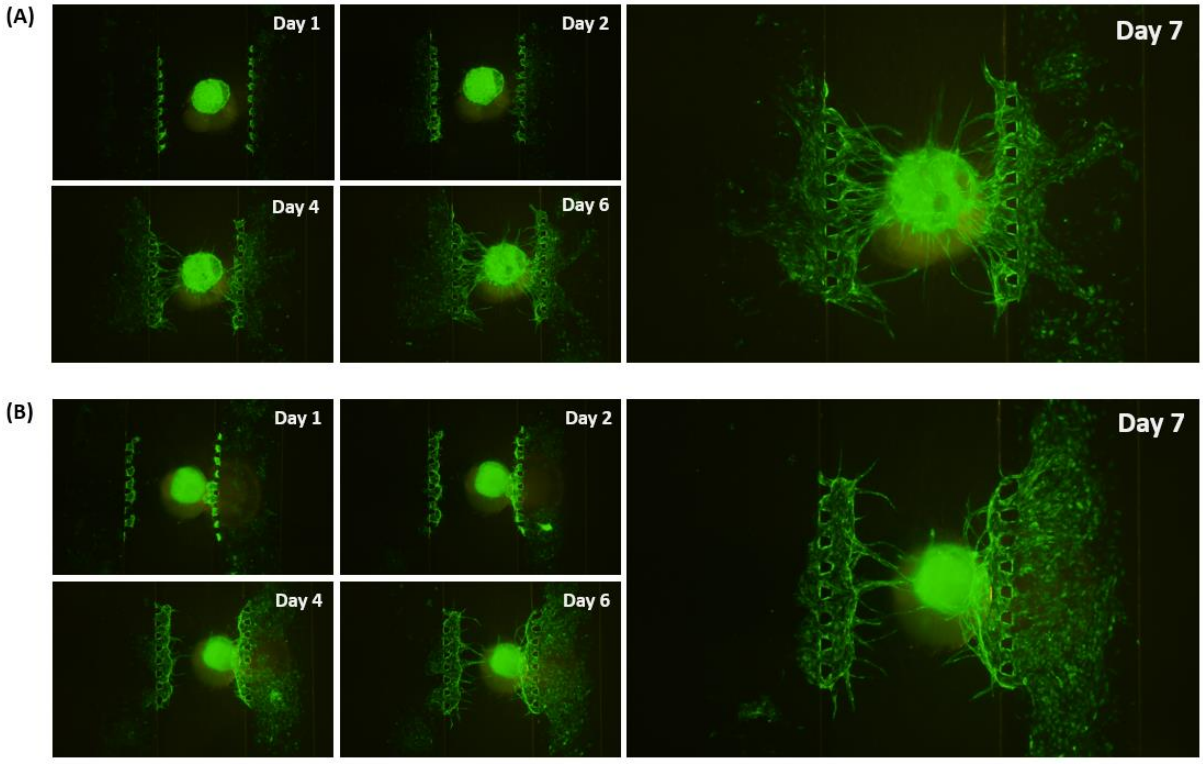

Figure 1. Fluorescence microscopy of vascular network formation in microfluidic device loaded with tumor spheroid. GFP-HUVECs (green color) was used to investigate vessel formation from day 1 to day 7 after spheroid seeding. (A) Tumor spheroid with perfusable vascular network (B) Tumor spheroid with non-perfusable vascular network.

2-3-c. E-selectin expression of tumor spheroid

Expression of E-selectin, together with CD31 as an endothelial cell marker, in monolayer cells and spheroids were evaluated in both presence and absence of inflammatory cytokines. **Figure 2A** indicated that nhLF and MCF-7 did not express E-selectin, whereas HUVECs expressed E-selectin at low level in resting stage and drastically increased the expression by more than thousand times in the presence of inflammatory cytokines.

CD31 was confirmed as a specific marker of HUVECs based on the results in **Figure 2B** showing that nhLF and MCF-7 did not express CD31. Despite inflammatory cytokines seemed to slightly lower CD31 expression of HUVECs in both monolayer and spheroid form, it was at most 15%. Therefore, change in expression of CD31 could be negligibly smaller than that of E-selectin. In case of the spheroid, expression of CD31 on day 3 was lower than on day 2. It is possibly due to slower proliferation rate of HUVECs (doubling time of ~48 h) than the other cells in spheroid such as MCF-7 cancer cells (doubling time of ~24 h). Since it was concerned that relative population of HUVEC in spheroids decreases with culture time, 2 days-old spheroid was used for loading into the microfluidic device. **Figure 2C** shows expression of E-selectin normalized with CD31 that is intrinsic to HUVECs. The ratio of E-selectin/CD31 was similar in both MCF-7-present and MCF-7-absent spheroids, indicating that MCF-7 did not enhance E-selectin expression of HUVECs in spheroid. However, addition of inflammatory cytokines greatly stimulated E-selectin expression regardless of monolayer or spheroid forms.

(A)

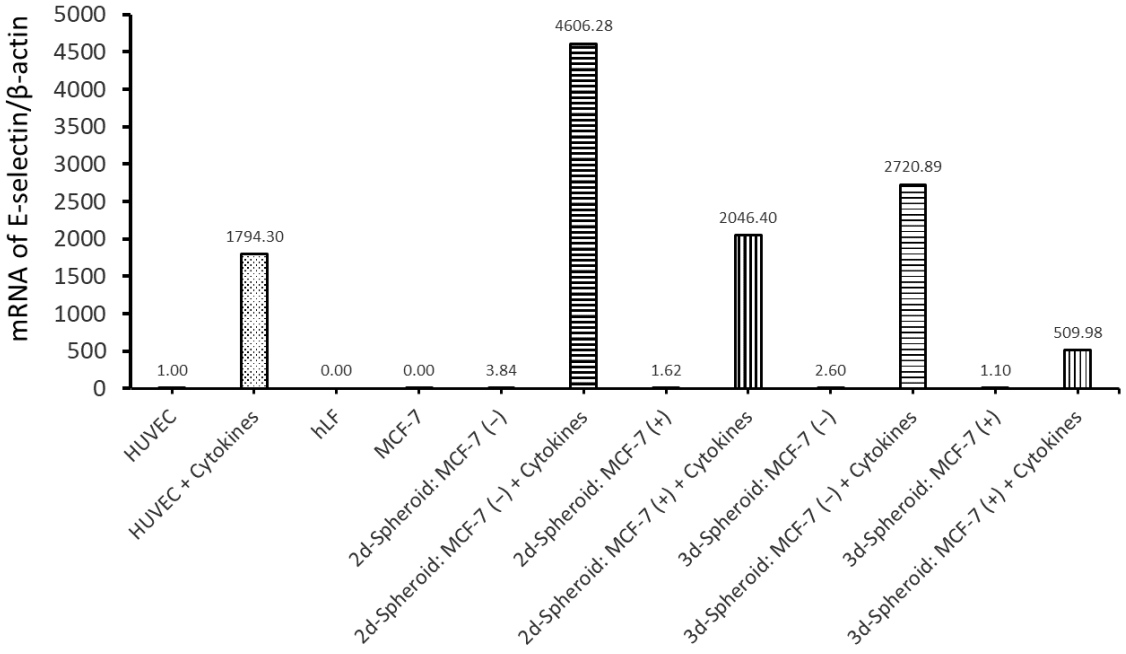

(B)

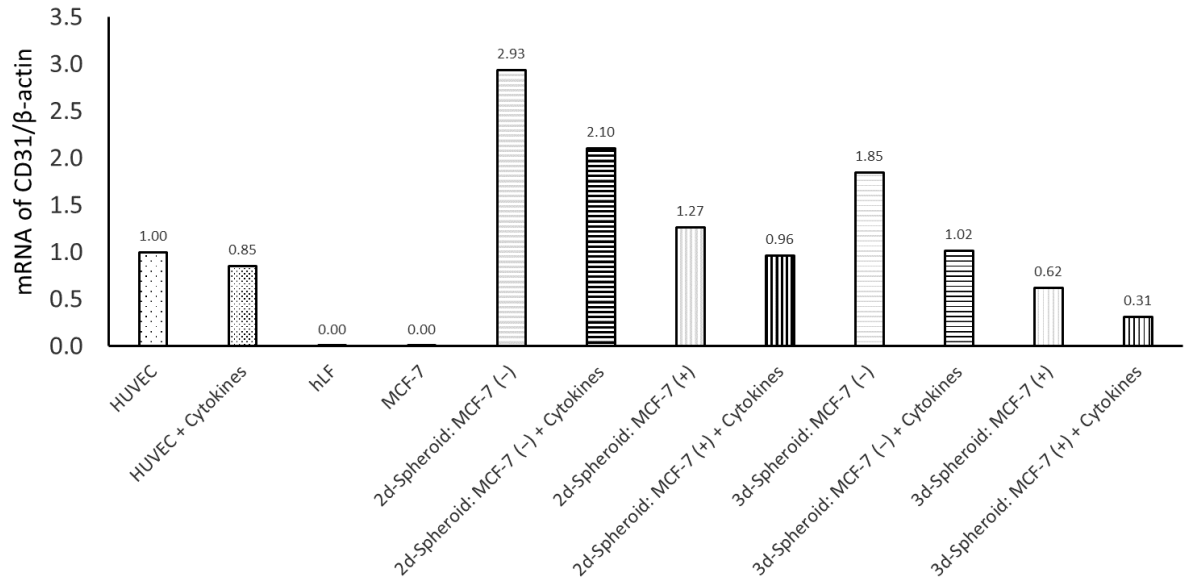

(C)

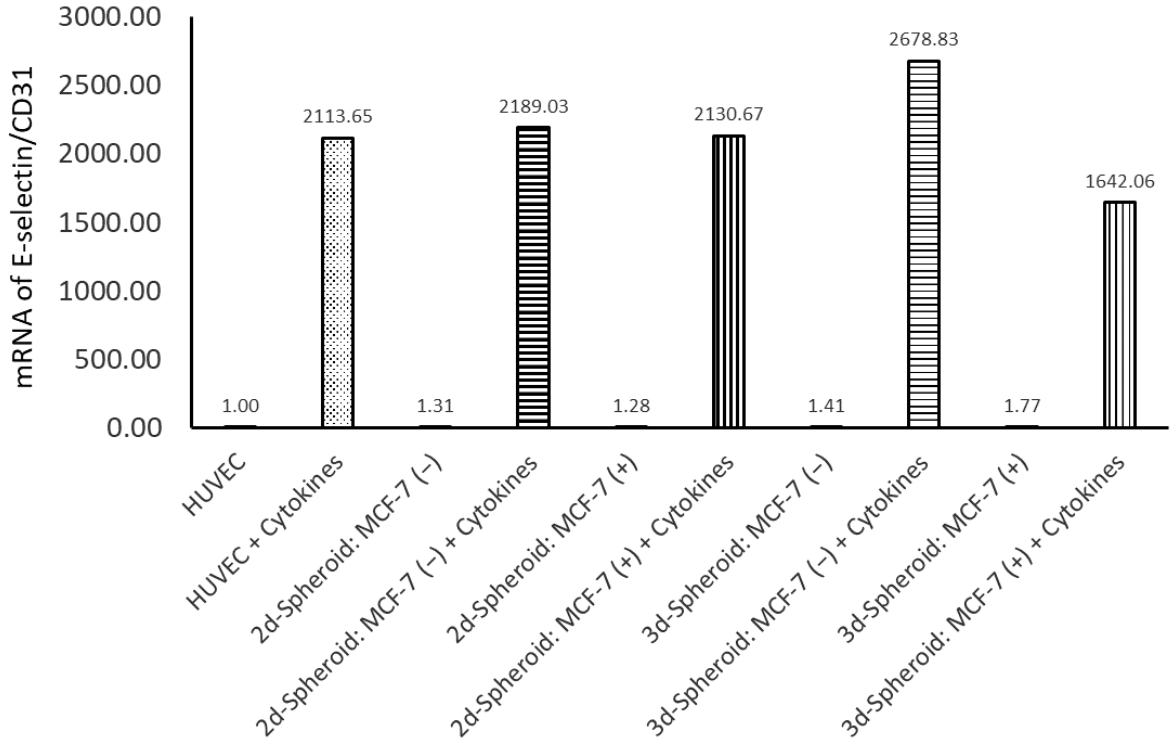

Figure 2. qRT-PCR for E-selectin expression of monolayer cells or spheroids in presence or absence of inflammatory cytokines. (A) mRNA of E-selectin normalized with mRNA of β-actin (B) mRNA of CD31, endothelial cells marker, normalized with mRNA of β-actin (C) mRNA of E-selectin/CD31, indicating E-selectin expressed by HUVECs.

2-3-d. Local disposition behavior of liposomes under dynamic flow condition

Using the tumor spheroid with perfusable vascular network, real-time imaging was done to uncover the local disposition behavior of fluorescent-labelled liposomes.

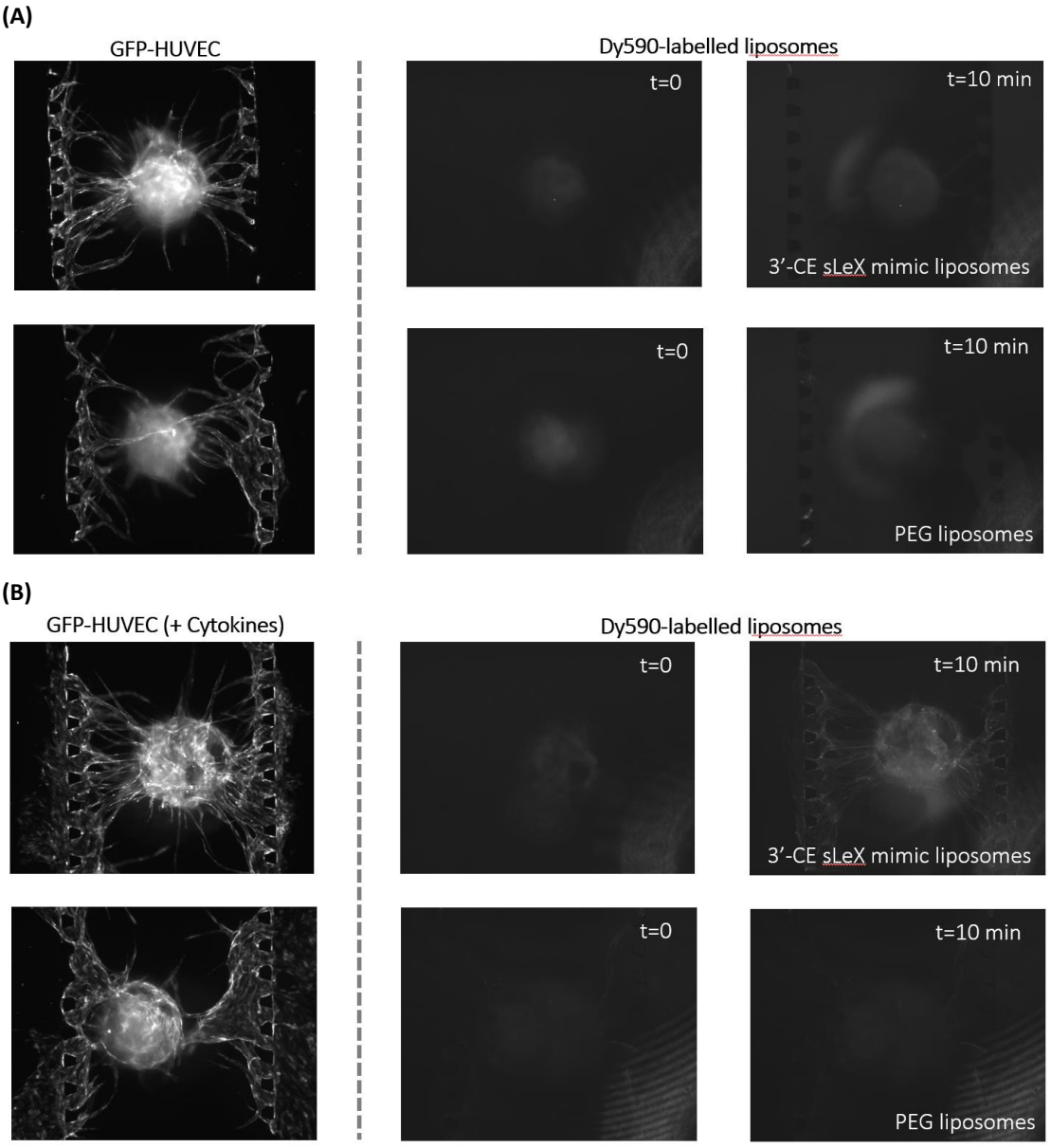

Figure 3. Real-time imaging of Dy590-labelled liposomes perfused in tumor spheroid for 10 min, image of GFP-HUVECs indicates perfusable vascular network formed by HUVECs (A) Tumor spheroid perfused with Dy590-labelled PEG liposomes or Dy590-labelled 3'-CE sLeX mimic liposomes. (B) Tumor spheroid with TNF-α and IL-1β pre-treatment for 4h before perfusion of Dy590-labelled PEG liposomes or Dy590-labelled 3'-CE sLeX mimic liposomes.

Figure 3A shows that 3'-CE sLeX mimic liposomes and PEG-liposomes had almost the same behaviour in tumor spheroid without cytokine treatment. In contrast, when the system was pretreated with inflammatory cytokines, significant amount of 3'-CE sLeX mimic

liposomes distributed along endothelial cells and their vicinity (**Figure 3B**). Since inflammatory cytokines induce E-selectin expression even in spheroid, the augmented uptake of 3'-CE sLeX mimic liposomes would be E-selectin-mediated. It would be interesting to visualize the interaction of 3'-CE sLeX mimic liposomes with endothelium under dynamic flow condition by using the vascularly perfusable spheroid.

2-4. Conclusion

A novel tumor vasculature model for evaluating the function of drug delivery systems was developed on microfluidic device. The tumor spheroid with perfusable vascular network can induce expression of E-selectin under the treatment with inflammatory cytokines, similarly to static 2D and 3D culture models. Only under the cytokine-treated condition, 3'-CE sLeX mimic liposomes, which can be strongly associated with E-selectin-expressing cells, were taken up much more greatly than PEG liposomes. Assuming that in vivo tumor endothelium exclusively expresses E-selectin, the 3'-CE sLeX mimic liposomes is a promising carrier for targeted drug delivery to tumor endothelium.

Chapter 3

Anti-angiogenic drug delivery to E-selectin expressing endothelial cells by using 3’-(1-carboxy)ethyl sialyl LewisX mimic liposomes

3-1. Introduction

Anti-angiogenic therapy is one of the most effective approaches for the treatment of various types of cancers; this therapy causes damage to the surrounding endothelial cells, which limits oxygen/nutrient supply to tumor cells and results in tumor necrosis. This advantage has led to many studies on anti-angiogenic drugs and their subsequent approval by the FDA for cancer therapy [97-99]. However, anti-angiogenic therapy may induce adaptive tumor microenvironmental defense mechanisms, leading to drug resistance or invasion [100, 101]. While combinatorial therapies using different drug targets are suggested to overcome the resistance [100, 101], attention has also been paid to targeted drug delivery to improve the efficacy of drugs in anti-angiogenic therapy [102]. For example, nanoparticles coated with collagen IV-binding peptides [103] or cyclic RGD peptides [104] were delivered to tumor endothelial cells, thereby improving the anti-tumorigenic and anti-metastatic activity of cytotoxic drugs in tumor-bearing mice. It has also been demonstrated that paclitaxel conjugated with factor VIIa, which binds to tissue factors expressed aberrantly in the tumor endothelium, suppresses tumor growth in paclitaxel-resistant cancer and inhibits its metastasis [105].

Everolimus (EVE) is an mTOR (mammalian target of rapamycin) inhibitor, which inhibits complex formation of serine/threonine kinase (mTOR) to raptor and mLST8 by binding to the cyclophilin FK binding protein-12. mTOR is generally activated in cancers and plays important roles in multiple cellular processes, especially tumor-relevant angiogenesis, endothelial cell proliferation, survival, and migration [106-110]. While several studies showed that EVE inhibits angiogenesis and tumor growth in tumor models [111, 112], the low bioavailability and low water solubility of the drug have limited its use. There have been attempts to overcome these drawbacks through the use of liposomes or nanocarriers [113-115].

Previous chapters have indicated that 3'-CE sLeX mimic liposomes appeared promising for the delivery of drugs to inflamed and tumor endothelial cells. In this chapter, EVE-encapsulated 3'-CE sLeX mimic liposomes were prepared and their capability in delivering drugs to E-selectin-expressing endothelial cells was evaluated. Using HUVECs activated with inflammatory cytokines as a model of tumor endothelium [116-120], cellular uptake and pharmacological effects of the liposomes were investigated.

3-2. Materials and Methods

3-2-a. Preparation and characterization of EVE-loaded liposomes

EVE was purchased from Chem Scene (South Brunswick Township, NJ, USA) and ethanol were purchased from Nacalai Tesque (Kyoto, Japan). DSPC, Cholesterol, DSPE-PEG_{2000}, and 3'-CE sLeX mimic were from the same sources as in chapter 1 and 2. EVE-loaded liposomes were prepared by ethanol injection method [112]. DSPC (5.5 µmol), cholesterol (4 µmol), and DSPE-PEG or 3'-CE sLeX-DSPE-PEG (0.5 µmol) were dissolved in 1 mL ethanol heated to 70°C in a glass tube. Twenty-four microliters of dimethyl sulfoxide (Nacalai Tesque, Kyoto, Japan) containing 0.5 µmol EVE was added to the lipid solution and incubated for 3 min at 70°C. The mixture was rapidly added to 2 mL phosphate-buffered saline (PBS) (Nissui Pharmaceutical, Tokyo, Japan) in a glass vial and stirred at 70°C for 30 sec. The ethanol in the mixture was removed under reduced pressure using a centrifugal evaporator (SpeedVac Concentrator SPD131DDA, Thermo Fisher Scientific, Waltham, MA, USA). The suspension was sonicated in a bath-type sonicator (ASU-3M, AS ONE, Osaka, Japan) at 70°C for 10 min and then with a tip-type sonicator (Ultrasonic generator US 300, Nissei, Tokyo, Japan) at an intensity of 200 W for 4 min. The liposome solution was filtered through a 0.45-µm membrane filter (Cosmonice Filter W, Nacalai Tesque, Kyoto, Japan) and was purified using a PD-10 gel filtration column (GE Healthcare, Buckinghamshire, UK) equilibrated with PBS. The concentration of phospholipids in the eluate was determined using a Phospholipids C-test Wako (Wako Pure Chemical Industry, Osaka, Japan) and adjusted to a concentration of 0.2 mg total lipids/mL in water for measurement of the particle size and zeta potential of the liposomes in a Zetasizer Nano ZS (Malvern, Worcester, UK). An aliquot of the stock solution was diluted 40 times with methanol, vortexed for 3 min, and filtered using 0.45-µm membrane filter (Cosmonice Filter S, Nacalai Tesque, Kyoto, Japan). EVE entrapment efficiency of each liposome was determined using an HPLC system (Prominence UFLC, Shimadzu Corporation, Kyoto, Japan) equipped with a ZORBAX column (SB-C8 4.6 I.D. x 75 mm, 3.5 µm, Agilent Technologies, Santa Clara, CA, USA), which was maintained at 60°C. The mobile phase comprised distilled water with 0.1% trifluoroacetic acid and acetonitrile with 20 mM triethylamine and 0.156% trifluoroacetic acid (40:60 v/v) and was maintained at a flow rate of 1 mL/min. The wavelength of detection of EVE was set to 278 nm.

3-2-b. Cell culture

HUVECs were cultured in HuMedia-EG2 culture medium, according to the protocol supplied by the manufacturer (Kurabo Industry, Osaka, Japan). When the cells reached 70%–80% confluence, they were harvested using trypsin-EDTA, suspended in the culture medium, and plated on a dish. The rest of the cells was maintained in a flask for up to 3 generations. On day 1 after plating, the cells were pretreated with 100 ng/mL TNF-α (Life Technologies, Carlsbad, CA, USA) and 10 ng/mL IL-1β (Sigma-Aldrich, St. Louis, MO, USA) for 5 h, to induce E-selectin expression.

3-2-c. Cellular toxicity

HUVECs were plated at a density of 10,000 cells/0.1 mL in a 96-well plate. Following a 5-h cytokine treatment, the cells were treated with EVE or EVE-loaded liposomes at the indicated concentration. After incubating for 3 h, 10 µL of Cell Count Reagent SF (Nacalai Tesque, Kyoto, Japan) was added to the culture medium and the cells were incubated for 2 h. The cell viability was detected colorimetrically using BioTek Eon Microplate Spectrophotometer (Biotek, Winooski, VT, USA) at a wavelength of 450 nm.

3-2-d. Cellular uptake and inhibition by anti E-selectin antibody

HUVECs were plated at a density of 200,000 cells/mL in a 12-well plate. After cytokine treatment, EVE or EVE-loaded liposomes were added to the plates at a concentration equivalent to 1 µM EVE. Following incubation for the indicated time periods, the cells were washed with ice cold PBS, scraped off in 100 µL of 10 mM ammonium acetate buffer, and transferred to 1.5 mL tubes. One-hundred microliters of acetonitrile was added to the cell suspension and vortexed for 1 min. After centrifugation at 10000 $\times$ g for 5 min, the supernatant was collected and filtered with 0.45-µm membrane filter. EVE concentration was determined using an LC-MS/MS system (LC-MS-8030, Shimadzu Corporation, Kyoto, Japan). Separation of EVE was achieved on a COSMOSIL 5C18-MS-II column (4.6 mm I.D. x 150 mm, Nacalai Tesque, Kyoto, Japan), which was maintained at 40°C, using 10 mM ammonium acetate and acetonitrile (20:80, v/v) at al flow of 1.0 mL/min. A post column splitter 1:4 was installed before the MS interface. EVE was detected using the mass transition m/z 976.45 $\rightarrow$ 909.60. In contrast, the pellet from the cell lysate was dissolved in 50 µL RIPA buffer (20 mM Tris HCl, 150 mM NaCl, 1 mM EDTA, 1% Triton-X 100, 0.1% SDS, 0.1% Na-deoxycholate), and the protein concentration was measured using Pierce BCA protein assay kit (Thermo Scientific, Rockford, IL, USA) for normalization of cellular uptake.

3-2-e. Inhibition of cell migration

HUVECs were plated at a density of 200,000 cells/500 µL in a 4-well, 35-mm dish (Cellvis, Sunnyvale, CA). After cytokine treatment, the cell layer was scratched with a 200-µL pipette tip and the culture medium was replaced with medium containing EVE or EVE-loaded liposomes at a concentration equivalent to 1 µM EVE. Live cell imaging was performed every hour for 3 h at 10× magnification using TD (transmitted image) scanning by a confocal microscope (Nikon A1RMP/Ti-E/PFS, Nikon Instruments Inc., Melville, NY, USA) equipped with NIS-elements AR 4.13.00 software. The scratch wound area was determined using Fiji package implemented in ImageJ software. All images were converted to grayscale, and the edges were enhanced and sharpened by the Sobel method. After the threshold was set to obtain a binary image, the edges of wound area were detected with ImageJ's wand tool. The enclosed area was calculated and expressed as a percentage of initial scratch wound area.

3-2-f. Inhibition of capillary tube formation

Prior to cell seeding, 450 µL of Matrigel (Corning, Bedford, MA, USA) was added to each well in a 2-well chamber slide glass (Matsunami glass Industry, Osaka, Japan) and incubated at 37°C for 30 min. HUVECs were seeded at a density of 240,000 cells/800 µL and incubated at 37°C. Thirty minutes later, 800 µL of culture medium supplemented with 200 ng/mL TNF-α and 20 ng/mL IL-1β, and 10% Matrigel was added to the chamber well. Five hours later, the EVE or EVE-loaded liposomes at a concentration equivalent to 1 µM EVE were added and incubated for 5 h. The morphology of the cell culture was investigated under a microscope (Biozero, BZ-8100, Keyence Corporation, Osaka, Japan).

3-2-g. Inhibition of mTOR signaling pathway

HUVECs were plated at a density of 500,000 cells/2 mL in a 6-well plate. After cytokine treatment, the cells were treated with EVE or EVE-loaded liposomes at a concentration equivalent to 1 µM EVE and incubated at 37°C for 4 h. To stimulate mTOR signaling, 50 ng/mL human epidermal growth factor (hEGF, Cell Signaling Technology, Denver, MA, USA) was added 15 min before the end of incubation, and the cells were washed with ice cold PBS. Eighty microliters of RIPA buffer with Halt phosphatase and protease inhibitor (Thermo Fisher Scientific, Waltham, MA, USA) was added to lyse the cells and the cells lysate was collected with a cell scraper. After centrifugation at 18,000 × g at 4°C for 20 min, the supernatant was aliquoted and heat-treated at 95°C for 5 min. The protein concentration was measured using the Pierce BCA protein assay kit (Thermo Fisher Scientific, Waltham, MA). A 15 µg protein

aliquot of each sample was subjected to SDS-PAGE on a 12.5% Precast gel (SuperSep Ace, Wako Pure Chemical Industry, Osaka, Japan) and transferred to a PVDF membrane (Immobilon, Merck Millipore, County Cork, Ireland). The membrane was blocked using Tris-buffered saline containing 3% bovine serum albumin (BSA, Sigma Life Science, St. Louis, MO, USA) at 25°C for 1 h and stained with Phospho-p70 S6 kinase (Thr389) antibody (Cell Signaling Technology, Denver, MA, USA) at a concentration of 1:1,000 at 4°C for 14 h as the primary antibody, followed by treatment with horseradish peroxidase (HRP)-conjugated goat anti-rabbit immunoglobulin G at a concentration of 1:10,000 at 25°C for 1 h (Abcam, Cambridge, U.K.) as the secondary antibody. A β-actin antibody (Santa Cruz Biotechnology, Dallas, TX, USA) was used as loading control at a concentration of 1:10,000 at 25°C for 1 h. All antibodies were diluted in Tris-buffered saline containing 1% BSA. The protein was detected using chemiluminescent HRP substrate (Merck, Billerica, MA) and imaged using ImageQuant LAS 4000 (GE Life Sciences, Buckinghamshire, UK). The results were shown as ImageJ densitometry units relative to the control sample.

3-2-h. Intracellular distribution

Cy5.5-labeled 3’-CE sLeX mimic liposomes were prepared according to the hydration method reported in chapter 1. Briefly, DSPC, cholesterol, 3’-CE sLeX mimic-linked DSPE-PEG, and DSPE-PEG-Cy5.5 were mixed in chloroform-methanol (1:1) at the molar ratio of 55:39:5:1 and then dried under reduced pressure using a rotary evaporator and vacuum desiccator. The lipid film was swollen and was suspended in PBS at 65°C. The suspension was sonicated in a bath-type sonicator at 65°C for 10 min and with a tip-type sonicator for 3 min, and then extruded through a 100 nm pore membrane equipped in an extruder maintained at 65°C. The liposome solution was purified using a PD-10 gel filtration column. To evaluate the intracellular distribution of 3’-CE sLeX mimic liposomes, HUVECs were plated at a density of 40,000 cells/0.25 mL in an 8-well chamber slide. After cytokine treatment of the cells, 3’-CE sLeX mimic liposomes were added and incubated for 1-4 h. At 2 h before the end of each incubation period, LysoTracker Green DND-26 (Thermo Fisher Scientific, Waltham, MA) was added to yield a final concentration of 75 nM. At the end of incubation, the medium was replaced with fresh culture medium and the cells were observed using a confocal microscope. A Golgi-ID green assay kit (Enzo Life Sciences, Farmingdale, NY, USA) was also used to stain the Golgi bodies. The Golgi Green Detection Reagent at concentration of 0.25 nmol/ml was co-incubated with 3’-CE sLeX mimic liposomes in the last 30 min. The cells were washed once

with assay solution and once with fresh medium before observation under a confocal microscope (Nikon A1RMP/Ti-E/PFS, Nikon Instruments Inc., Melville, NY, USA) equipped with NIS-elements AR 4.13.00 software. The excitation wavelength was set at 488.5 and 637.3 nm, and the emission wavelengths were scanned in the range of 500−550 nm and 663–738 nm for FITC and Cy5.5, respectively.

3-3. Results and Discussion

3-3-a. Preparation and characterization of EVE-loaded liposomes

The ethanol injection method has been used to prepare EVE- or rapamycin-loaded liposomes and has provided liposomes with good characteristics [113, 121, 122]. The EVE-loaded liposomes prepared in this thesis were comparable in size and drug-to-lipid molar ratio to those in past reports [113, 123]. **Table 1** summarizes the particle size and zeta potential of the prepared liposomes. The average diameter was approximately 90 nm for both EVE/PEG- and EVE/3'-CE sLeX mimic liposomes. Their polydispersity indices were 0.17 and 0.20, indicating that both liposomes have an acceptably uniform size distribution. The EVE/3'-CE sLeX mimic liposome was highly negative with a zeta potential of −27.2 mV, whereas EVE/PEG-liposomes was slightly negative indicating a weaker surface charge. Total lipid recovery of both liposomes was more than 80% confirming no significant loss during preparation. The drug-to-lipid molar ratio of both liposomes was 0.016 and 0.017, which is comparable with 0.02 of the past studies [113].

Table 1. Characteristics of liposomes used in this study

Liposomes	Average diameter (nm)	Polydispersity index	Zeta potential (mV)	Total lipid recovery (%)	Drug-to-lipid molar ratio
EVE/PEG	90.12 ± 0.55	0.17	-13.83 ± 3.58	82.57	0.017
EVE/3'-CE sLeX mimic	92.93 ± 0.87	0.20	-27.20 ± 2.62	80.85	0.016
Cy5.5-labeled 3'-CE sLeX mimic	87.98 ± 0.90	0.09	-27.43 ± 1.52	93.21	-

Results of diameter and zeta potential are expressed as mean ± SD of three samples.

3-3-b. Cellular toxicity

WST-8 assay was carried out to evaluate the cellular toxicity of plain and liposomal EVE and determine the dose used for cellular uptake and anti-angiogenic studies. **Figure 1** shows percent viability of cytokine-treated HUVECs following treatment at different

concentrations of the drugs for 3 h. Regardless of treatment with plain or liposomal EVE, the cell viability was more than 80% at concentrations of up to 1 μM. Therefore, 1 μM EVE was chosen for further studies to ensure minimal cell death during the experiment. The designated concentration was consistent with past studies [111, 115] that had investigated an inhibitory effect of EVE on angiogenesis-related endothelial functions in HUVECs.

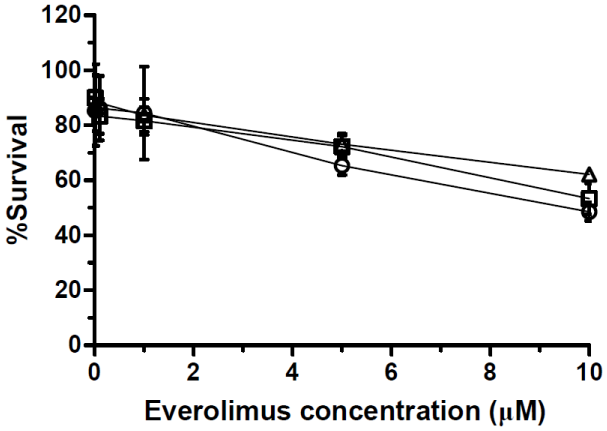

Figure 1. WST-8 assay for cellular toxicity of EVE or EVE-loaded liposomes in HUVECs treated with TNF-α and IL-1β. Following 5-h cytokine pretreatment, the cells were incubated with plain or liposomal EVE for 3 h and with WST-8 reagent for an additional 2 h. Symbols: □, plain EVE; △, EVE/PEG-liposomes; ○, EVE/3'-CE sLeX mimic liposomes. Results are expressed as mean ± SD of three samples.

3-3-c. Cellular uptake

The uptake of plain or liposomal EVE in HUVECs treated with proinflammatory cytokines was investigated. As shown in **Figure 2**, cellular uptake of EVE was the highest with plain EVE, followed by EVE/3'-CE sLeX mimic liposomes, and then EVE/PEG-liposomes. When plain EVE was administered, the uptake appeared to reach a plateau within almost 1 h. The relatively rapid equilibrium achieved with plain EVE is associated with the mechanism of simple diffusion across the plasma membrane in accordance with the lipophilic nature of EVE. In contrast, the uptake of EVE/3'-CE sLeX mimic liposomes increased steadily over 3 h and almost caught up with plain EVE. As reported in chapter 1 that fluorescein-labeled 3'-CE sLeX mimic liposomes have been taken up by E-selectin-mediated endocytotic processes, the specialized process involving cytotic membrane transport could be slower than simple diffusion of small lipophilic molecules. The uptake of EVE/3'-CE sLeX mimic liposomes was significantly higher than that of EVE/PEG-liposomes, but the difference between the two liposome formulations was not so large as that seen with fluorescein-labeled liposomes in chapter 1. Leakage of EVE from liposomes could not be ruled out.

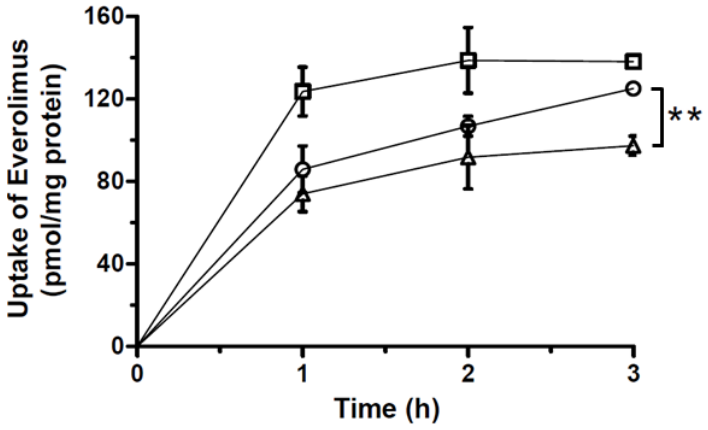

Figure 2. Time-courses of the uptake of EVE or EVE-loaded liposomes in HUVECs treated with TNF-α and IL-1β. Following 5-h cytokine pretreatment, the cells were incubated with plain or liposomal EVE for 1–3 h. The amount of EVE associated with the cells was determined by LC-MS/MS and normalized with cellular protein content. Symbols: □, plain EVE; △, EVE/PEG-liposomes; ○, EVE/3'-CE sLeX mimic liposomes. Results are expressed as mean ± SD of three samples. **P<0.01

To clarify the involvement of the E-selectin-mediated uptake process, the effect of anti-E-selectin antibody on cellular uptake was investigated. As shown in **Figure 3**, the uptake of EVE/3'-CE sLeX mimic liposomes was significantly inhibited in the presence of anti-E-selectin antibody, whereas it was not observed with either EVE/PEG-liposomes or plain EVE. Interestingly, the uptake of EVE/3'-CE sLeX mimic liposomes under antibody blockade was comparable to that of EVE/PEG-liposomes, implying that the release of EVE from liposome formulations, if any, was not different between the two. Therefore, the improved uptake of EVE/3'-CE sLeX mimic liposomes would be primarily due to an E-selectin-mediated uptake process.

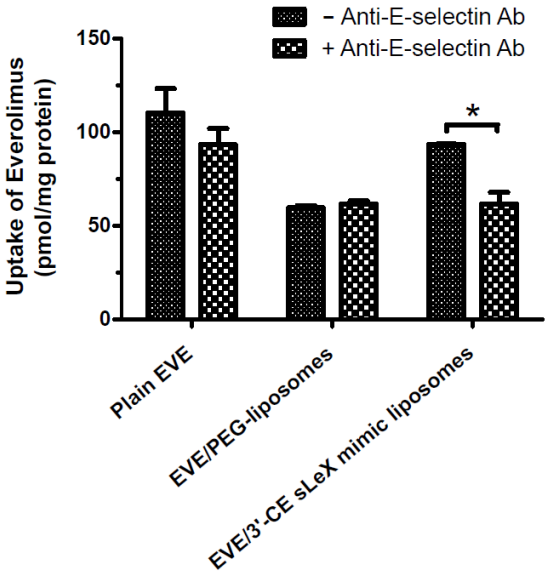

Figure 3. Inhibition of the uptake of EVE-loaded liposomes by anti-E-selectin antibody in HUVECs treated with TNF-α and IL-1β. Following pretreatment with cytokines for 5 h, anti-Eselectin antibody was added in some groups to block E-selectin to yield a final concentration of 10 μg/mL. After 30 min, plain or liposomal EVE were added, and the cells were incubated for 1 h. The amount of EVE associated with the cells was determined by LC-MS/MS and normalized with cellular protein content. Results are expressed as mean + SD of three samples. *P<0.05.

3-3-d. Anti-angiogenic effect

The main endothelial functions involved in angiogenesis are cell migration and capillary tube formation. Cell migration plays an important role in the initial steps of angiogenesis, starting with basement membrane break down and followed by mitosis and migration in response to angiogenic factors including VEGF. After migration, endothelial cells initiate tube formation and develop new vessels to complete angiogenesis [124, 125]. To investigate the anti-angiogenic effect of plain and liposomal EVE, a scratch assay and capillary tube formation were conducted. Moreover, the regulation of the mTOR cascade was confirmed by the degree of Thr389 phosphorylation of pS6 kinase (Ser235/236).

Migration of cytokine-treated HUVECs in the presence of EVE or EVE-loaded liposomes was evaluated in a scratch assay. **Figure 4** shows the percentage of wound closure within 3h incubation with EVE or EVE-loaded liposomes. The control cells, i.e., HUVECs treated with TNF-α and IL-1β, showed 36.2% wound closure within 3 h. However, treatment with plain EVE and EVE/3'-CE sLeX mimic liposomes suppressed the wound closure by more than half (12% and 15.5%, respectively). The suppressive effect of EVE/PEG-liposomes was moderate, resulting in 24.3 % wound closure. These trends regarding suppression of cell migration were in agreement with cellular uptake of EVE from each formulation.

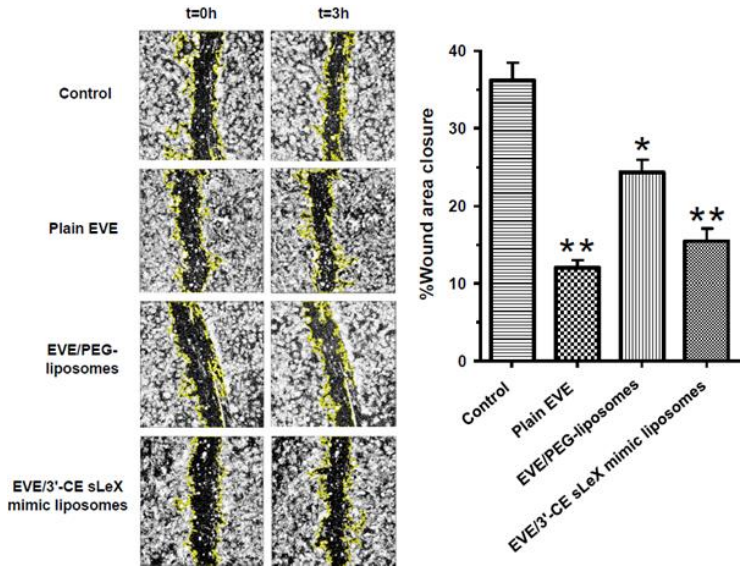

Figure 4. Effect of EVE or EVE-loaded liposomes on migration of HUVECs treated with TNF-α and IL-1β within a time period of 3 h. After cytokine treatment, the cell layers were scratched with a pipette tip and incubated with 1 μM plain or liposomal EVE. Live cell imaging was performed every hour for 3 h under a confocal microscope. The scratch wound area was computed from digitalized images on ImageJ platform. The data represent a percentage of wound closure against an initial scratch wound area. Results are expressed as mean + SD of three samples. *P<0.05, **P<0.01 comparing to control.

Tube formation assay is another popular in vitro method to evaluate angiogenesis. Endothelial progenitor cells such as HUVECs form tubes when placed on a 3D extracellular matrix. **Figure 5** shows the effect of plain EVE and EVE-loaded liposomes on tube formation. Formation of tubes and networks from cytokine-treated HUVECs was significantly inhibited by plain EVE and EVE/3'-CE sLeX mimic liposomes after 5 h of exposure, whereas the EVE/PEG-liposomes did not significantly interrupt the formation.

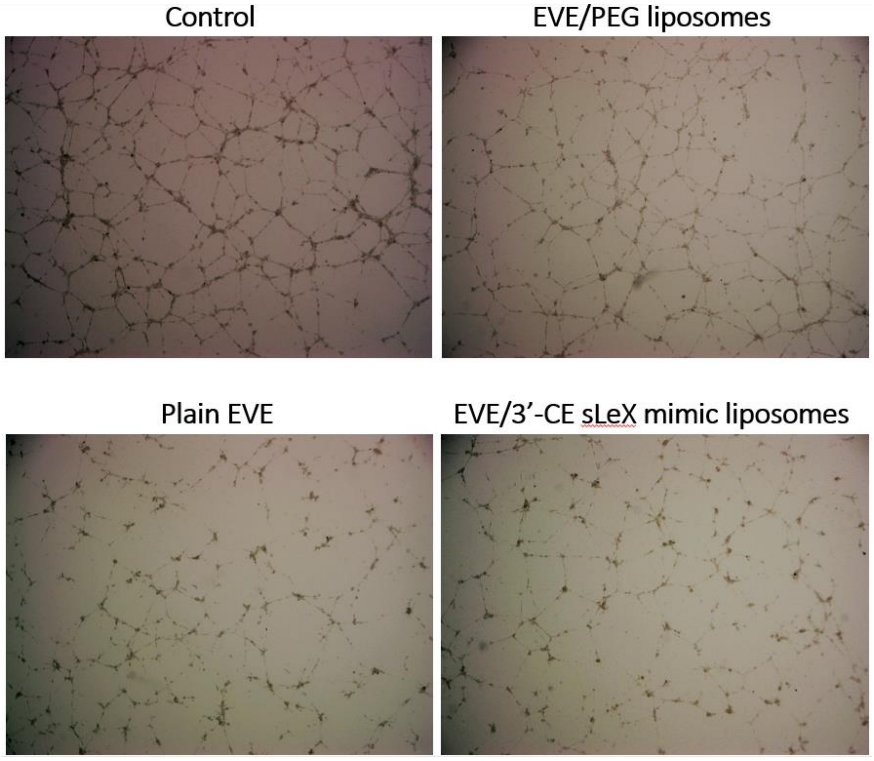

Figure 5. Effect of EVE or EVE-loaded liposomes on tube formation in HUVECs treated with TNF-α and IL-1β. HUVECs were plated on Matrigel and treated with proinflammatory cytokines for 5 h. The cells were treated with 1 μM plain or liposomal EVE for 5 h and observed under a microscope.

Western blot analysis was performed to confirm phosphorylation of pS6 kinase at Thr389 amino acid residues, which is a downstream target of EVE in the mTOR signaling pathway [126]. Phosphorylation of pS6 kinase was induced by EGF according to the method described by Damiano V, et al. [111], in addition to TNF-α and IL-1β [127-129]. As shown in **Figure 6**, treatment with plain EVE and EVE/3'-CE sLeX mimic liposomes remarkably suppressed phosphorylation of pS6 kinase to less than the endogenous level. EVE/PEG-liposomes suppressed phosphorylation of p70 S6 kinase but not that of p85 S6 kinase. p85 S6 kinase is a splicing variant of p70 S6 kinase, having 23 extra amino acids at the amino-terminus. Since the additional peptide sequence encodes a nuclear localizing signal, p85 S6 kinase is

exclusively localized in the nuclei [127, 130, 131]. The difference in subcellular localization or protein structure between the two S6 kinases might relate to the differential suppression of phosphorylation observed with EVE/PEG-liposomes, which could be emphasized only when the suppressive effect was mild. Nevertheless, a high correlation between cellular uptake, cell migration, tube formation, and phosphorylation of pS6 kinases implied that not only plain EVE but liposomal EVE are likely to suppress angiogenesis via mTOR signaling pathway.

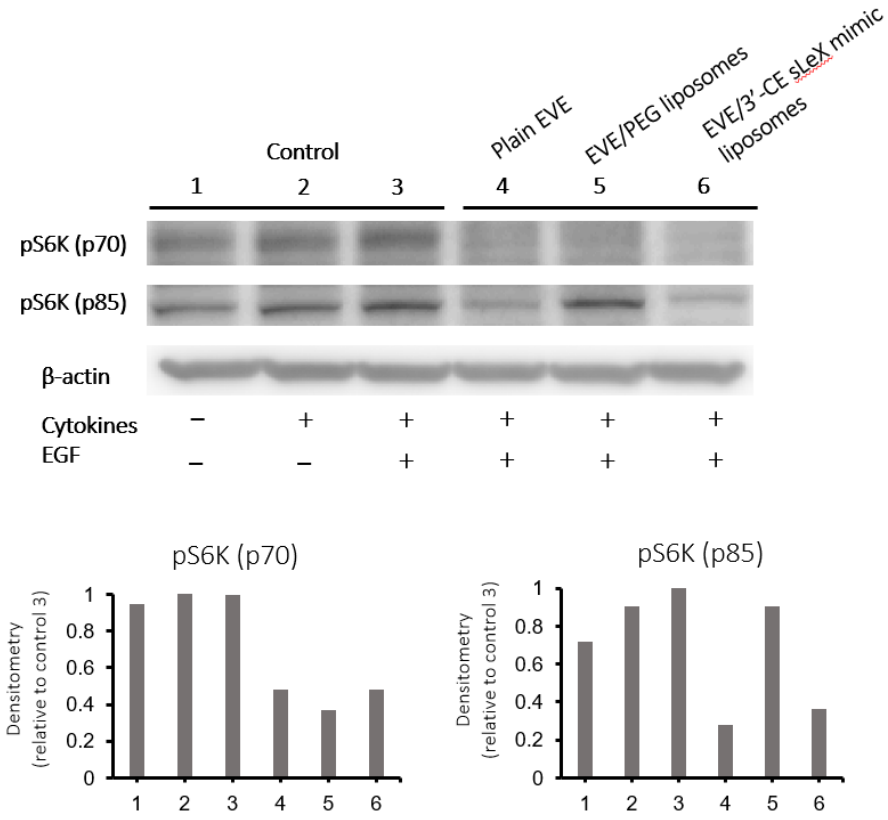

Figure 6. Effect of EVE or EVE-loaded liposomes on phosphorylation of pS6 kinase in HUVECs treated with TNF-α and IL-1β. Following pretreatment with cytokines for 5 h, the cells were incubated with 1 μM plain or liposomal EVE for 4 h. The cells were treated with 50 ng/mL hEGF for the last 15 min, lysed with RIPA buffer, and subjected to western blotting using antiphospho- p70 S6 kinase antibody.

3-3-e. Intracellular distribution

Considering the uncertain observation that E-selectin-targeted liposomes are transported intracellularly via clathrin-independent pathways followed by transport to the Golgi bodies and endoplasmic reticulum [14] or the endosome/lysosome pathway followed by release in the cytoplasm [22, 23], intracellular disposition behavior of 3'-CE sLeX mimic liposomes was also investigated.

Confocal fluorescence microscopy was employed to clarify subcellular distribution of fluorescence-labeled 3’-CE sLeX mimic liposomes. As shown in **Figure 7**, red fluorescence signal associated with 3’-CE sLeX mimic liposomes increased over time. The images indicating such gradual uptake of 3’-CE sLeX mimic liposomes corresponded to the result of quantification of EVE by LC-MS/MS (**Figure 2**), as well as uptake results in chapter 1. The intracellular study in chapter 1 was not conclusive in terms of subcellular localization of the liposomes because of low resolution and no subcellular staining, but **Figure 7** clearly indicates that the liposomes appear to be transported preferentially to lysosomes than to the Golgi bodies. Taking all findings together, it was suggested that EVE/3’-CE sLeX mimic liposomes are taken up and disassembled in an endosome/lysosome pathway, leading to the release of EVE in the cytoplasm. Results that sLeX-liposomes are not directly transported to the nucleus are in agreement with the conclusion of Stahn et al. [132].

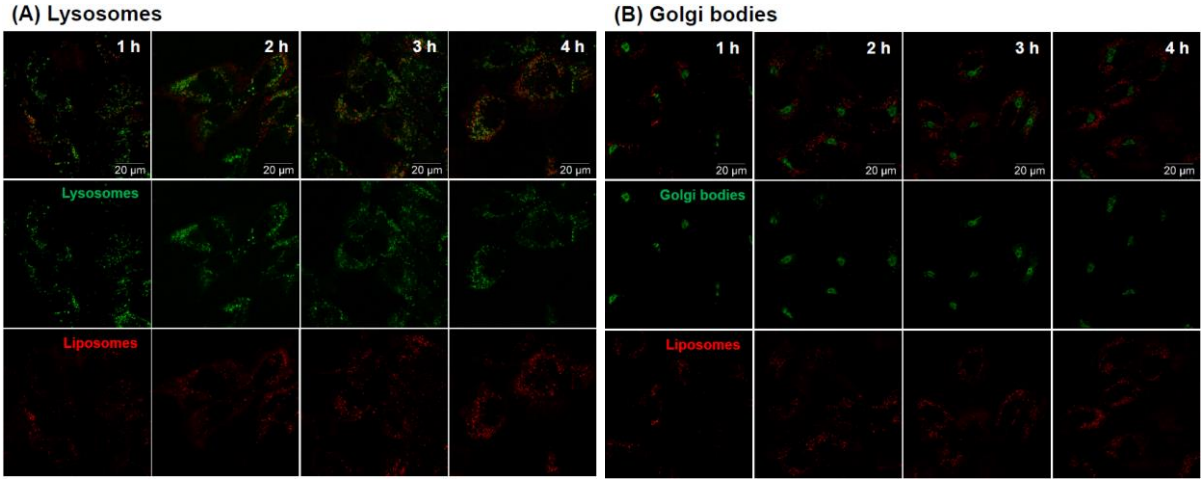

Figure 7. Confocal microscopy of subcellular distribution of Cy5.5-labeled 3’-CE sLeX mimic liposomes in HUVECs treated with TNF-α and IL-1β. Subcellular distribution of 3’-CE sLeX mimic liposomes (red color) was investigated following the staining of lysosomes (A) and Golgi bodies (B) with LysoTracker Green DND-26 and Golgi-ID green assay kit, respectively. The images were taken after 1–4 h of treating the cells with the liposomes.

3-4. Conclusion

EVE/3’-CE sLeX mimic liposomes were intracellularly taken up by E-selectin and prompted an anti-angiogenic effect of EVE involved in the mTOR signaling pathway. However, the effectiveness of 3’-CE sLeX mimic liposomes was limited in case of the delivery of EVE, presumably due to moderate retention of the drug. The drug delivery potential of 3’-CE sLeX mimic liposomes and the formulations of EVE need to be further investigated and optimized.

Summary

The aim of this study was to develop E-selectin-targeted liposomes, by design of novel structurally simplified sLeX mimics as ligands, for delivering drugs to inflamed endothelium including tumor vasculature. The findings of each chapter are summarized as follows

Chapter 1: Development and functional characterization of liposomes decorated with structurally simplified sLeX mimics

Structurally simplified novel sLeX analogs were designed and linked with DSPE-PEG for E-selectin-mediated liposomal delivery. The sLeX structural simplification strategies include (1) replacement of the Gal-GlcNAc disaccharide unit with lactose to reduce many initial steps and (2) substitution of neuraminic acid with a negatively charged group, i.e., 3'-sulfo, 3'-carboxymethyl (3'-CM), or 3'-(1-carboxy)ethyl (3'-CE). While all the liposomes developed were similar in particle size and charge, the 3'-CE sLeX mimic liposome showed the highest uptake mediated primarily by E-selectin in inflammatory cytokine-treated HUVECs, being even more potent than native sLeX-decorated liposomes. MD simulation studies demonstrated that the 3'-CE sLeX mimic is more strongly bound to E-selectin than native sLeX, because of the higher probability of hydrogen-bond formation. Therefore, the 3'-CE sLeX mimic liposome has a greater potential for targeted drug delivery to the endothelium of inflamed tissues.

Chapter 2: Transport characteristics of 3’-(1-carboxy)ethyl sialyl LewisX mimic liposomes in tumor spheroids with a perfusable vascular network

Tumor spheroids with a perfusable vascular network were prepared in microfluidic device as tumor vasculature model that allows to analyze the local disposition behavior of liposomes in solid tumors. The endothelial cells in the spheroid formed a continuous vascular network with angiogenic sprouts branchedly elongated from open microchannels of the device. Treatment with TNF-α and IL-1β could increase E-selectin expression in tumor spheroid. Perfusion study of fluorescent-labeled liposomes shows that 3’-CE sLeX mimic liposomes significantly distributed along endothelial cells and their vicinity in the spheroid under flow condition. In contrast, control pegylated liposomes showed low retention due to weak binding. These results suggested that 3’-CE sLeX mimic liposomes were taken up in perfused tumor spheroid much higher than PEG liposomes. Therefore, the 3’-CE sLeX mimic liposomes has a potential for targeted drug delivery to tumor endothelium.

Chapter 3: Anti-angiogenic drug delivery to E-selectin expressing endothelial cells by using 3'-(1-carboxy)ethyl sialyl LewisX mimic liposomes

Everolimus-encapsulated 3'-CE sLeX mimic liposomes (EVE/3'-CE sLeX mimic liposomes) was developed and evaluated in inflammatory cytokines-treated HUVECs. The uptake of EVE in 3'-CE sLeX mimic liposomes increased steadily and almost caught up with the uptake of plain EVE at 3 h, which was higher than that in PEG liposomes. The improved uptake was confirmed as E-selectin-mediated endocytotic processes. However, the difference between the uptake of the two liposome formulations was not so large, leakage of EVE from liposomes could not be ruled out. Cell migration and capillary tube formation of HUVECs, referring to their angiogenic activity, were suppressed significantly by the EVE/3'-CE sLeX mimic liposomes compared to the control. Thr389 phosphorylation of pS6 kinase, as a marker of mTOR activity, was remarkably suppressed to less than endogenous levels by EVE/3'-CE sLeX mimic liposomes. These studies demonstrated that EVE/3'-CE sLeX mimic liposomes were intracellularly taken up by E-selectin and prompted anti-angiogenic effects of EVE involved in the mTOR signaling pathway. However, moderate retention of EVE in the liposomes might limit the targeting ability of 3'-CE sLeX mimic liposomes.

In conclusion, the novel structurally simplified sLeX mimic-decorated liposomes were successfully developed as a potential carrier to deliver drugs targeting to inflamed endothelium including tumor vasculature.

Acknowledgement

My five years in Japan have been the most challenging years of my life. Obtaining my Master's degree and Doctoral Degree would not have been possible without the guidance, support, and help of wonderful people that I have met throughout this journey. I would like to express my sincerest gratitude to the following:

To Professor Emeritus Mitsuru Hashida (Institute for Advanced Study, Kyoto University) for accepting me to this laboratory and giving me many opportunities in my student life.

To Professor Fumiyoshi Yamashita (Graduate School of Pharmaceutical Sciences, Kyoto University) for his supervision, great ideas in research, and constructive discussion. I learned a lot of doctoral skills from him that will surely help me in my future career.

To Senior Assistant Professor Yuriko Higuchi (Graduate School of Pharmaceutical Sciences, Kyoto University) for her guidance, advice, continuous support, and valuable discussion. I have learned many experiment skills from her that will certainly help me work smoothly in my researcher life.

To Professor Hiromune Ando (Center for Highly Advanced Integration of Nano and Life Sciences (G-CHAIN), Gifu University) and Associate Professor Akiharu Ueki (Faculty of Pharmaceutical Sciences, Aomori University) for their support in synthesis. This thesis would not be complete without their help.

To Professor Isao Nakanishi (Faculty of Pharmacy, Kindai University) and Assistant Professor Shinya Nakamura (Faculty of Pharmacy, Kindai University) for providing Molecular dynamic simulation, which really helped improve this thesis.

To Associate Professor Ryuji Yokokawa (Faculty of Engineering, Kyoto University) and Dr. Ryu Okada (Faculty of Engineering, Kyoto University) for their support in spheroid development, which is very important for this thesis, their hospitality, and their encouraging words.

To the Japanese Government and MEXT for the financial support. I hope they would continue providing opportunities to others like me who want to pursue their graduate studies in Japan.

To my lab mates for their assistance in my experiments and my Japanese friends for helping me with matters in Japanese that I do not understand.

To my Thai friends for making my life in a foreign country less difficult and enjoyable.

To those who wish me all good things that I cannot mention all here, thank you.

To my family - my mom Sarin, my brother Issara, and my family in the Philippines and Australia - for their unconditional love, prayers, encouraging, and wishes. They gave me strength to overcome all obstacles. My success and achievements are for you.

To my husband, Jason, for being by my side in every situation, supporting me the best in both physical and mental health, making my life better and happier, helping, caring, and loving me unconditionally.

Finally, to Gods for blessing me and being my spiritual anchor.

List of Publications

Synthesis and functional characterization of novel sialyl LewisX mimic-decorated liposomes for E-selectin-mediated targeting to inflamed endothelial cells.

Chanikarn Chantarasrivong, Akiharu Ueki, Ryutaro Ohyama, Johan Unga, Shinya Nakamura, Isao Nakanishi, Yuriko Higuchi, Shigeru Kawakami, Hiromune Ando, Akihiro Imamura, Hideharu Ishida, Fumiyoshi Yamashita, Makoto Kiso, Mitsuru Hashida.

Molecular Pharmaceutics. 2017. 14, 1528-1537.

Disposition behaviors of sialyl LewisX mimic-decorated liposomes in tumor spheroids with a perfusable vascular network.

Chanikarn Chantarasrivong, Ryu Okada, Yuriko Higuchi, Miku Konishi, Naoko Komura, Hiromune Ando, Ryuji Yokokawa, Fumiyoshi Yamashita.

Manuscript in preparation

Sialyl LewisX mimic-decorated liposomes for anti-angiogenic everolimus delivery to E-selectin expressing endothelial cells.

Chanikarn Chantarasrivong, Yuriko Higuchi, Masahiro Tsuda, Mitsuru Hashida, Miku Konishi, Naoko Komura, Hiromune Ando, Fumiyoshi Yamashita.

Manuscript in preparation

References

1. Ehrhardt, C.; Kneuer, C.; Bakowsky, U. Selectins-an emerging target for drug delivery. Adv. Drug Delivery Rev. 2004, 56, 527-549.
2. Zhang, J.; Alcaide, P.; Liu, L.; Sun, J.; He, A.; Luscinskas, F. W.; Shi, G. P. Regulation of Endothelial Cell Adhesion Molecule Expression by Mast Cells, Macrophages, and Neutrophils. PLoS One 2011, 6, e14525.
3. Ray, K. P.; Farrow, S.; Daly, M.; Talabot, F.; Searle, N. Induction of the E-selectin promoter by interleukin 1 and tumour necrosis factor alpha, and inhibition by glucocorticoids. Biochem. J. 1997, 328, 707-715.
4. Narita, T.; Kimura, N. K.; Kasai, Y.; Hosono, J.; Nakashio, T.; Matsuura, N.; Sato, M.; Kannagi, R. Induction of E-selectin expression on vascular endothelium by digestive system cancer cells. J. Gastroenterol. 1996, 31, 299-301.
5. Eichbaum, C.; Meyer, A. S.; Bischofs, E.; Steinborn, A.; Bruckner, T.; Brodt, P.; Sohn, C.; Eichbaum, M. H. R. Breast cancer cell-derived cytokines, macrophages and cell adhesion: Implications for metastasis. Anticancer Res. 2011, 31, 3219-3228.
6. Khatib, A. M.; Kontogiannea, M.; Fallavollita, L.; Jamison, B.; Meterissian, S.; Brodt, P. Rapid induction of cytokine and E-selectin expression in the liver in response to metastatic tumor Cells. Cancer. Res. 1999, 59, 1356-1361.
7. Ma, S.; Tian, X. Y.; Zhang, Y.; Mu, C.; Shen, H.; Bismuth, J.; Pownall, H. J.; Huang, Y.; Wong, W. T. E-selectin-targeting delivery of microRNAs by microparticles ameliorates endothelial inflammation and atherosclerosis. Sci. Rep. 2016, 6, 22910.
8. Kang, H. W.; Josephson, L.; Petrovsky, A.; Weissleder, R.;Bogdanov, A. Magnetic resonance imaging of inducible E-selectin expression in human endothelial cell culture. Bioconjugate Chem. 2002, 13, 122-127.
9. Barthel, S. R.; Gavino, J. D.; Descheny, L.; Dimitroff, C. J. Targeting selectins and selectin ligands in inflammation and cancer. Expert Opin. Ther. Targets 2007, 11, 1473-1491.
10. Bhaskar, V.; Law, D. A.; Ibsen, E.; Breinberg, D.; Cass, K. M.; Dubridge, R. B.; Evangelista, F.; Henshall, S. M.; Hevezi, P.; Miller, J. C.; Pong, M.; Powers, R.; Senter, P.; Stockett, D.; Sutherland, R. L.; Jeffry, U. V.; Willhite, D.; Murray, R.; Afar, D. E. H.; Ramakrishnan, V. E Selectin up-regulation allows for targeted drug delivery in prostate cancer. Cancer. Res. 2003, 63, 6387-6394.

11. Kuznetsova, N. R.; Stepanova, E. V.; Peretolchina, N. M.; Khochenkov, D. A.; Boldyrev, I. A.; Bovin, N. V.; Vodovozova, E. L. Targeting liposomes loaded with melphalan prodrug to tumour vasculature via the Sialyl Lewis X selectin ligand. J. Drug Target. 2014, 22, 242-250.
12. Vodovozova, E. L.; Moiseeva, E. V.; Grechko, G. K.; Gayenko, G. P.; Nifant'ev, N. E.; Bovin, N. V.; Molotkovsky, J. G. Antitumour activity of cytotoxic liposomes equipped with selectin ligand SiaLex, in a mouse mammary adenocarcinoma model. Eur. J. Cancer 2000, 36, 942-949.
13. DeFrees, S. A.; Phillips, L.; Guo, L.; Zalipsky, S. Sialyl Lewis X liposomes as a multivalent ligand and inhibitor of E-selectin mediated cellular adhesion. J. Am. Chem. Soc. 1996, 118, 6101-6104.
14. Alekseeva, A.; Kapkaeva, M.; Shcheglovitova, O.; Boldyrev, I.; Pazynina, G.; Bovin, O.; Vodovozova, E. Interactions of antitumour sialyl Lewis X liposomes with vascular endothelial cells. Biochim. Biophys. Acta, Biomembr. 2015, 1848, 1099-1110.
15. Minaguchi, J.; Oohashi, T.; Inagawa, K.; Ohtsuka, A.; Ninomiya, Y. Transvascular accumulation of Sialyl Lewis X conjugated liposome in inflamed joints of collagen antibody-induced arthritic (CAIA) mice. Arch. Histol. Cytol. 2008, 71, 195-203.
16. Zalipsky, S.; Mullah, N.; Harding, J. A.; Gittelman, J.; Guo, L.; DeFrees, S. A. Poly(ethylene glycol)-grafted liposomes with oligopeptide or oligosaccharide ligands appended to the termini of the polimer chains. Bioconjugate Chem. 1997, 8, 111-118.
17. Danishefsky, S. J.; Gervay, J.; Peterson, J. M.; McDonald, F. E.; Koseki, K.; Griffith, D. A.; Oriyama, T.; Marsden, S. P. Application of glycols to the synthesis of oligosaccharides: convergent total syntheses of the Lewis X trisaccharide Sialyl Lewis X antigenic determinant and higher congeners. J. Am. Chem. Soc. 1995, 117, 1940-1953.
18. Ellervik, U.; Magnusson, G. A high yielding chemical synthesis of Sialyl Lewis X tetrasaccharide and Lewis X trisaccharide; examples of regio- and sterio differentiated glycosylations. J. Org. Chem. 1998, 63, 9314-9322.
19. Palcic, M. M.; Venot, A. P.; Ratcliffe, R. M.; Hindsgaul, O. Enzymic synthesis of oligosaccharides terminating in the tumor associated Sialyl-Lewis-a determitant. Carbohydr. Res. 1989, 190, 1-11.

20. Ball, G. E.; O'Neill, R. A.; Schultz, J. E.; Lowe, J. B.; Weston, B. W.; Nagy, J. O.; Brown, E.G.; Hobbs, C. J.; Bednarski, M. D. Synthesis and structural analysis using 2-D NMR of Sialyl Lewis X (SLex) and Lewis X (Lex) oligosaccharides: ligands related to E-selectin [ELAM-1] binding. J. Am. Chem. Soc. 1992, 114, 5449-5451.
21. Bendas, G.; Krause, A.; Schmidt, R.; Vogel, J.; Rothe, U. Selectins as new targets for immunoliposome-mediated drug delivery: A potential way of anti-inflammatory therapy. Pharm. Acta. Helv. 1998, 73, 19-26.
22. Kessner, S.; Krause, A.; Rothe, U.; Bendas, G. Investigation of the cellular uptake of E-selectin-targeted immunoliposomes by activated human endothelial cells. Biochim. Biophys. Acta. 2001, 1514, 177-190.
23. Spragg, D. D.; Alford, D. R.; Greferath, R.; Larsen, C. E.; Lee, K. D.; Gurtner, G. C.; Cybulsky, M. I.; Tosi, P. F.; Nicolau, C.; Gimbrone Jr. M. A. Immunotargeting of liposomes to activated vascular endothelial cells: a strategy for site-selective delivery in the cardiovascular system. Proc. Natl. Acad. Sci. U.S.A. 1997, 94, 8795-8800.
24. Dickerson, J. B.; Blackwell, J. E.; Ou, J. J.; Shinde Patil, V. R.; Goetz, D. J. Limited adhesionof biodegradable microspheres to E- and P-selectin under flow. Biotechnol. Bioeng. 2001, 73, 500-509.
25. Blackwell, J. E.; Dagia, N. M.; Dickerson, J. B.; Berg, E. L.; Goetz, D. J. Ligand coated nanosphere adhesion to E- and P-selectin under static and flow conditions. Ann. Biomed. Eng. 2001, 29, 523-533.
26. Hashida, N.; Ohguroa, N.; Yamazakib, N.; Arakawac, Y.; Oikid, E.; Mashimoa, H.; Kurokawae, N.; Tanoa, Y. High-efficacy site-directed drug delivery system using sialyl-Lewis X conjugated liposome. Exp. Eye. Res. 2008, 86, 138-149.
27. Jubeli, E.; Moine, L.; Nicolas, V.; Barratt, G. Preparation of E-selectin-targeting nanoparticles and preliminary in vitro evaluation. Int. J. Pharm. 2012, 426, 291-301.
28. Ding, Y.; Li, S.; Nie, G. Nanotechnological strategies for therapeutic targeting of tumor vasculature. Nanomedicine. 2013, 8, 1209-1222.
29. Kasterena, S. I.; Campbellb, S. J.; Serresc, S.; Anthonyb, D. C.; Sibsonc, N. R.; Davisa, B. G. Glyconanoparticles allow pre-symptomatic in vivo imaging of brain disease. PNAS. 2009, 106, 18-23.

30. Harding, J. A.; Engbers, C. M.; Newman, M. S.; Goldstein, N. I.; Zalipsky, S. Immunogenicity and pharmacokinetic attributes of poly(ethylene glycol)-grafted immunoliposomes. Biochim. Biophys. Acta. 1997, 1327, 181-192.
31. Mann, A. P.; Tanaka, T.; Somasunderam, A.; Liu, X.; Gorenstein, D. G.; Ferrari, M. E-selectin-targeted porous silicon particle for nanoparticle delivery to the bone marrow. Adv. Mater. 2011, 23, 278-82.
32. Zalipsky, S.; Mullah, N.; Harding, J. A.; Gittelman, J.; Guo, L.; DeFrees, S. A. Poly(ethylene glycol)-grafted liposomes with oligopeptide or oligosaccharide ligands appended to the termini of the polimer chains. Bioconjug. Chem. 1997, 8, 111-118.
33. Danishefsky, S. J.; Gervay, J.; Peterson, J. M.; McDonald, F. E.; Koseki, K.; Griffith, D. A.; Oriyama, T.; Marsden, S. P. Application of glycals to the synthesis of oligosaccharides: convergent total syntheses of the Lewis X trisaccharide Sialyl Lewis X antigenic determinant and higher congeners. J. Am. Chem. Soc. 1995, 117, 1940-1953.
34. Ellervik, U.; Magnusson, G. A high yielding chemical synthesis of Sialyl Lewis X tetrasaccharide and Lewis X trisaccharide; examples of regio- and sterio differentiated glycosylations. J. Org. Chem. 1998, 63, 9314-9322.
35. Palcic, M. M.; Venot, A. P.; Ratcliffe, R. M.; Hindsgaul, O. Enzymic systhesis of oligosaccharides terminating in the tumor-associated Sialyl-Lewis-a determitant. Carbohydr. Res. 1989, 190, 1-11.
36. Neelu, K.; Bert, E. T. Design and Synthesis of Sialyl Lewisx Mimics as E- and P-Selectin Inhibitors. Med. Res. Rev. 2002, 22, 566-601.
37. Titz, A.; Patton, J.; Smiesko, M.; Radic, Z.; Schwardt, O.; Magnani, J. L.; Ernst, B. Probing the carbohydrate recognition domain of E-selectin: The importance of the acid orientation in sLex mimetics. Bioorg. Med. Chem. 2010, 18, 19-27.
38. Graves, B. J.; Crowther, R. L.; Chandran, C.; Rumberger, J. M.; Li, S.; Huang, K. S.; Presky, D. H.; Familletti, P. C.; Wolitzky, B. A.; Burns, D. K. Insight into E-selectin/ligand interaction from the crystal structure and mutagenesis of the lec/EGF domains. Nature. 1994, 367, 532-538.
39. Somers, W. S.; Tang, J.; Shaw, G. D.; Camphausen, R. T. Insights into the Molecular Basis of Leukocyte Tethering and Rolling Revealed by Structures of P- and E-Selectin Bound to SLeX and PSGL-1. Cell. 2000, 103, 467-479.

40. Preston, R. C.; Jakob, R. P.; Binder, F. P. C.; Sager, C. P.; Ernst, B.; Maier, T. E-selectin ligand complexes adopt an extended high-affinity conformation. J. Mol. Cell. Biol. 2016, 8, 62-72.

41. Wong, C. H.; Varas, F. M.; Hung, S. C.; Marron, T. G.; Lin, C. C.; Gong, K. W.; Schmidt, G. W. Small molecules as structural and functional mimics of Sialyl Lewis X tetrasaccharide in Selectin inhibition: A remarkable enhancement of inhibition by additional negative charge and/or hydrophobic Group. J. Am. Chem. Soc. 1997, 119, 8152-8158.

42. Simanek, E. E.; McGarvey, G. J.; Jablonowski, J. A.; Wong, C. H. Selectin-carbohydrate interactions: from natural ligands to designed mimics. Chem. Rev. 1998, 98, 833-862.

43. Sakagami, M.; Hotie, K.; Higashi, K.; Yamada, H.; Hamana, H. Syntheses and evaluation of biantennary oligosaccharide ligands mimicking Sialyl Lewis X. Chem. Pharm. Bull. 1999, 47, 1237-1245.

44. Brandley, B. K.; Kiso, M.; Abbas, S.; Nikrad, P.; Srivasatava, O.; Foxall, C.; Oda, Y.; Hasegawa, A. Structure-function studies on selectin carbohydrate ligands. Modifications to fucose, sialic acid and sulphate as a sialic acid replacement. Glycobiology. 1993, 3, 633-641.

45. Ohmoto, H.; Nakamura, K.; Inoue, T.; Kondo, N.; Inoue, Y.; Yoshino, K.; Kondo, H.; Ishida, H.; Kiso, M.; Hasegawa, A. Studies on selectin blocker. 1. structure-activitiy relationships of Sialyl Lewis X analogs. J. Med. Chem. 1996, 39, 1339-1343.

46. Rao, B. N.; Anderson, M. B.; Musser, J. H.; Gilbert, J. H.; Schaefer, M. E.; Foxall, C.; Brandley, B. K. Sialyl Lewis X mimics derived from a pharmacophore search are Selectin inhibitors with anti-inflammatory activity. J. Biol. Chem. 1994, 269, 19663-19666.

47. Papahadjopoulos, D.; Allen, T. M.; Gabizon, A.; Mayhew, E.; Matthay, K.; Huang, S. K.; Lee, K. D.; Woodle, M. C.; Lasic, D. D.; Redemann, C.; Martin, F. J. Sterically stabilized liposomes: improvements in pharmacokinetics and antitumor therapeutic efficacy. Proc. Natl. Acad. Sci. 1991, 88, 11460-11464.

48. Yamaoka, T.; Tabata, Y.; Ikada, Y. Distribution and tissue uptake of poly(ethylene glycol) with different molecular weights after intravenous administration to mice. J. Pharm. Sci. 1994, 83, 601-606.

49. Allen, T. M.; Hansen, G.; Martin, F.; Redeman, C.; Yau-Young, A. Liposomes containing synthetic lipid derivatives of poly(ethyleneglycol) show prolonged circulation half-lives in vivo. Biochim. Biophys. Acta. 1991, 1066, 29-36.
50. Klibanov, A. L.; Maruyama, K.; Torchilin, V. P.; Huang, L. Amphipathic polyethylene glycols effectively prolong the circulation time of liposomes. FEBS. Lett. 1990, 268, 235-237.
51. Jubeli, E.; Moine, L.; Gauduchon, J. V.; Barratt, G. E-selectin as a target for drug delivery and molecular imaging. J. Control. Release. 2012, 158, 194-206.
52. Wang, Y.; Yan, Q.; Wu, J.; Zhang, L. H.; Ye, X. S. A new one-pot synthesis of α-Gal epitope derivatives involved in the hyperacute rejection response in xenotransplantation. Tetrahedron. 2005, 61, 4313-43121.
53. Ishiwata, A.; Munemura, Y.; Ito, Y. Synergistic solvent effect in 1,2-cis-glycoside formation. Tetrahedron. 2008, 64, 92-102.
54. GROMACS version 5.0.4. http://www.gromacs.org/
55. Hornak, V.; Abel, R.; Okur, A.; Strockbine, B.; Roitberg, A.; Simmerling C. Comparison of multiple amber force fields and development of improved protein backbone parameters. Proteins. 2006, 65, 712-725.
56. Wang, J.; Wolf, R. M.; Caldwell, J. W. ; Kollman, P. A. ; Case III, D. A. Development and testing of a general amber force field. J. Comput. Phys. 2004, 25, 1157-1174.
57. Jakalian, A.; Bush, B. L.; Jack D. B.; Bayly C.I. Fast, efficient generation of high-quality atomic charges. AM1-BCC model: I. Method. J. Comp. Chem. 2000, 21, 132-146.
58. Jorgensen, W. L. Quantum and statistical mechanical studies of liquids. 10. Transferable intermolecular potential functions for water, alcohols, and ethers. Application to liquid water. J. Am. Chem. Soc. 1981, 103, 335-340.
59. Lu, D.; Hu, Y.; He, X.; Sollogoub, M.; Zhang, Y. Total synthesis of a sialyl Lewisx derivative for the diagnosis of cancer. Carbohydr. Res. 2014, 383, 89-96.
60. Chapman, P. T.; Yarwood, H.; Harrison, A. A.; Stocker, C. J.; Jamar, F.; Gundel, R. H.; Peters, A. M.; Haskard, D. O. Endothelial activation in monosodium urate monohydrate crystal-induced inflammation. In vitro and in vivo studies on the roles of tumor necrosis factor α and interleukin-1. Arthritis. Rheum. 1997, 40, 955-965.
61. Matharu, N. M.; Butler, L. M.; Rainger, G. E.; Gosling, P.; Vohra, R. K.; Nash, G. B. Mechanisms of the anti-inflammatory effects of hydroxyethyl starch

demonstrated in a flow-based model of neutrophil recruitment by endothelial cells. Crit. Care. Med. 2008, 36, 1536-1542.

62. Boyle, E. M. Jr.; Kovacich, J. C.; Canty, T. G. Jr.; Morgan, E. N.; Chi, E.; Verrier, E. D.; Pohlman, T. H. Inhibition of nuclear factor-kappa B nuclear localization reduces human E-selectin expression and the systemic inflammatory response. Circulation. 1998, 98, 282-288.
63. Onat, D.; Brillon, D.; Colombo, P. C.; Schmidt, A. M. Human vascular endothelial cells: A model system for studying vascular inflammation in diabetes and atherosclerosis. Curr. Diab. Rep. 2011, 11, 193-202.
64. Kim, I.; Moon, S. O.; Park, S. K.; Chae, S. W.; Koh, G. Y. Angiopoietin-1 reduces VEGF-stimulated leukocyte adhesion to endothelial cells by reducing ICAM-1, VCAM-1, and E-selectin expression. Circ. Res. 2001, 14, 477-479.
65. Wada, Y.; Saito, T.; Matsuda, N.; Ohmoto, H.; Yoshino, K.; Ohashi, M.; Kondo, H. Studies on selectin blockers. 2. Novel selectin blocker as potential therapeutics for inflammatory disorders. J. Med. Chem. 1996, 39, 2055-2059.
66. Rodgers, S. D.; Camphausen, R. T.; Hammer, D. A. Sialyl Lewis(x)-mediated, PSGL-1-independent rolling adhesion on P-selectin. Biophys. J. 2000, 79, 694-706.
67. Malý, P.; Thall, A. D.; Petryniak, B.; Rogers, C. E.; Smith, P. L.; Marks, R. M.; Kelly, R. J.; Gersten, K. M.; Cheng, G.; Saunders, T, L.; Camper, S. A.; Camphausen, R. T.; Sullivan, F. X.; Isogai, Y.; Hindsgaul, O.; Andrian, U. H.; Lowe, J. B. The α(1,3) Fucosyltransferase Fuc-TVII Controls Leukocyte Trafficking through an Essential Role in L-, E-, and P-selectin Ligand Biosynthesis. Cell. 1996, 86, 643-653.
68. Shodai, T.; Suzuki, J.; Kudo, S.; Itoh, S.; Terada, M.; Fujita, S. Shimazu, H.; Tsuji, T. Inhibition of P-selectin-mediated cell adhesion by a sulfated derivative of sialic acid. Biochem. Biophys. Res. Commun. 2003, 312, 787-793.
69. Yao, L.; Pan, J.; Setiadi, H.; Pate1, K. D.; McEver, R. P. Interleukin 4 or Oncostatin M induces a prolonged increase in P-Selectin mRNA and protein in Human endothelial cells. J. Exp. Med. 1996, 184, 81-92.
70. Foreman, K. E.; Vaporciyan, A. A.; Bonish, B. K.; Jones, M. L.; Johnson, K. J.; Glovsky, M. M.; Eddy, S. M.; Ward, P. A. C5a-induced expression of P-selectin in endothelial cells. J. Clin. Invest. 1994, 94, 1147-1155.
71. Thoma, G.; Magnani, J. L.; Patton, J. T. Synthesis and biological evaluation of a Sialyl Lewis X mimic with significantly improved E-selectin inhibition. Bioorg. Med. Chem. Lett. 2001, 11, 923-925.

72. Hanessian, S.; Reddy, G. V.; Huynh, H. K.; Pan, J.; Pedatella, S. Design and synthesis of sialyl Lex mimetics based on carbocyclic scaffolds derived from (–) quinic acid. Bioorg. Med. Chem. Lett. 1997, 7, 2729-2734.
73. Li, F.; Wilkins, P. P.; Crawley, S; Weinstein, J.; Cummings, R. D.; McEve, R. P. Post-translational modifications of recombinant P-selectin glycoprotein ligand-1 required for binding to P- and E-selectin. J. Biol. Chem. 1996, 271, 3255-3264.
74. Siemann, D. W.; Horsman, M. R. Vascular targeted therapies in oncology. Cell. Tissue. Res. 2009, 335, 1, 241-248.
75. Hanahan, D.; Weinberg, R. A. Hallmarks of cancer: the next generation. Cell. 2011, 144, 5, 646-74.
76. Chen, F.; Cai, W. Tumor Vasculature Targeting: A Generally Applicable Approach for Functionalized Nanomaterials. Small. 2014, 10, 1887-1893.
77. Wittig, C.; Scheuer, C.; Parakenings, J.; Menger, M. D.; Laschke, M. W. Geraniol Suppresses Angiogenesis by Downregulating Vascular Endothelial Growth Factor (VEGF)/VEGFR-2 Signaling. PLoS ONE. 2015, 10, 7, e0131946.
78. Kurohane, K.; Tominaga, A.; Sato, K.; North, J. R.; Namba, Y.; Oku, N. Photodynamic therapy targeted to tumor-induced angiogenic vessels. Cancer Lett. 2001, 167, 49-56.
79. Takeuchi, Y.; Kurohane, K.; Ichikawa, K.; Yonezawa, S.; Nango, M.; Oku, N. Induction of Intensive Tumor Suppression by Antiangiogenic Photodynamic Therapy Using Polycation-Modified Liposomal Photosensitizer. Cancer. 2003, 97, 8, 2027-2034.
80. Ohkouchi, K.; Imoto, H.; Takakura, Y.; Hashida, M.; Sezaki, H. Disposition of Anticancer Drugs after Bolus Arterial Administration in a Tissue-isolated Tumor Perfusion System. Cancer Res. 1990, 50, 1640-1644.
81. Biel, N. M.; Lee, J. A.; Sorg, B. S.; Siemann, D. W. Limitations of the dorsal skinfold window chamber model in evaluating anti-angiogenic therapy during early phase of angiogenesis. Vascular Cell. 2014, 6, 17, 1-11.
82. Staton, C. A.; Reed, M. W.; Brown, N. J. A critical analysis of current in vitro and in vivo angiogenesis assays. Int. J. Exp. Path. 2009, 90, 195-221.
83. Pampaloni, F.; Reynaud, E. G.; Stelzer, E. H. K. The third dimension bridges the gap between cell culture and live tissue. Nat. Rev. Mol. Cell Biol. 2007, 8, 10, 839-845.

84. Shamir, E. R.; Ewald, A. J. Three-dimensional organotypic culture: experimental models of mammalian biology and disease. Nat. Rev. Mol. Cell Biol. 2014, 15, 10, 647-664.
85. Fennema, E.; Rivron, N.; Rouwkema, J.; Blitterswijk, C.; Boer, J. Spheroid culture as a tool for creating 3D complex tissues. Trends in Biotechnology. 2013, 31, 2, 108-115.
86. Lin, R. Z.; Chang, H. Y. Recent advances in three-dimensional multicellular spheroid culture for biomedical research. Biotechnol. J. 2008, 3, 1172-1184.
87. Mehta, G.; Hsiao, A. Y.; Ingram, M.; Luker, G. D.; Takayama, S. Opportunities and Challenges for use of Tumor Spheroids as Models to Test Drug Delivery and Efficacy. J Control Release. 2012, 164, 2, 192-204.
88. Kim, S.; Lee, H.; Chung, M.; Jeon, N. L. Engineering of functional, perfusable 3D microvascular networks on a chip. Lab. Chip. 2013, 13, 8, 1489-1500.
89. Moya, M. L.; Hsu, Y. H.; Lee, A. P.; Hughes, C. C. W.; George, S. C. In Vitro Perfused Human Capillary Networks. Tissue Eng. Part C Methods. 2013, 19, 9, 730-737.
90. Nashimoto, Y.; Hayashi, T.; Kunita, I.; Nakamasu, A.; Torisawa, Y.; Nakayama, M.; Imamura, H. T.; Kotera, H.; Nishiyama, K.; Miura, T.; Yokokawa, R. Integrating perfusable vascular networks with a three-dimensional tissue in a microfluidic device. Integr. Biol. 2017, 9, 506-518.
91. Nashimoto, Y.; Teraoka, Y.; Banan Sadeghian, R.; Nakamasu, A.; Arima, Y,; Hanada, S.; Kotera, H.; Nishiyama, K.; Miura, T.; Yokokawa, R. Perfusable Vascular Network with a Tissue Model in a Microfluidic Device. J. Vis. Exp. 2018, 134, e57242.
92. Newman, A. C.; Nakatsu, M. N.; Chou, W.; Gershon, P. D.; Hughes, C. C. W. The requirement for fibroblasts in angiogenesis: fibroblast-derived matrix proteins are essential for endothelial cell lumen formation. Mol. Biol. Cell. 2011, 22, 3791-3008.
93. Nashimoto, Y.; Hanada, S.; Arima, Y.; Kotera, H.; Nishiyama, K.; Miura, T.; Yokokawa, R. On-chip vascular network for the culture of three-dimensional tissue model. Presentation in Keystone symposia on molecular and cellular biology, organs- and tissues-on-chips, Montana, USA. 8-12 April 2018.
94. Zang, H. Thin-Film Hydration Followed by Extrusion Method for Liposome Preparation. Methods Mol. Biol. 2017, 1522, 17-22.
95. Konerding, M. A.; Fait, E.; Gaumann, A. 3D microvascular architecture of pre-cancerous lesions and invasive carcinomas of the colon. Br. J. Cancer. 2001, 84, 1354-1362.

96. Siemann, D. W. The Unique Characteristics of Tumor Vasculature and Preclinical Evidence for its Selective Disruption by Tumor-Vascular Disrupting Agents. Cancer Treat Rev. 2011, 37, 1, 63-74.
97. Li, T.; Kang, G.; Wang, T.; Huang, H. Tumor angiogenesis and anti-angiogenic gene therapy for cancer. Oncol. Lett. 2018, 16, 687-702.
98. Dutour, A.; Rigaud, M. Tumor endothelial cells are targets for selective therapies: in vitro and in vivo models to evaluate antiangiogenic strategies. Anticancer Res. 2005, 25, 3799-3808.
99. Samant, R. S.; Shevde, L. A. Recent advances in anti-angiogenic therapy of cancer. Onco. Target. 2011, 2, 122-134.
100. Bergers, G.; Hanahan, D. Modes of resistance to anti-angiogenic therapy. Nat. Rev. Cancer. 2008, 8, 592-603.
101. Ma, S.; Pradeep, S.; Hu, W.; Zhang, D.; Coleman, R.; Sood, A. The role of tumor microenvironment in resistance to anti-angiogenic therapy. F1000 Res. 2018, 326, 7, 1-19.
102. Abdalla, A. M. E.; Xiao, L.; Ullah, M. W.; Yu, M.; Ouyang, C.; Yang, G. Current challenges of cancer anti-angiogenic therapy and the promise of nanotherapeutics. Theranos. 2018, 8, 2, 533–548.
103. Tan, F.; Mo, X. H.; Zhao, J.; Liang, H.; Chen, Z. J.; Wang, X. L. A novel delivery vector for targeted delivery of the antiangiogenic drug paclitaxel to angiogenic blood vessels: TLTYTWS-conjugated PEG–PLA nanoparticles. J. Nanopart. Res. 2017, 19, 51.
104. Murphy, E. A.; Majeti, B. K.; Barnes, L. A.; Makale, M.; Weis, S. M., Lutu-Fuga, K.; Wrasidlo, W.; Cheresh, D.A. Nanoparticle-mediated drug delivery to tumor vasculature suppresses metastasis. Proc. Natl. Acad. Sci. USA. 2008, 105, 9343-9348.
105. Zhu, S.; Kisiel, W.; Lu, Y. J.; Petersen, L. C.; Ndungu, J. M.; Moore, T. W.; Parker, E. T.; Sun, A.; Liotta, D. C.; El-Rayes, B. F.; Brat, D. J.; Snyder, J. P.; Shoji, M. Tumor angiogenesis therapy using targeted delivery of paclitaxel to the vasculature of breast cancer metastases. J. Drug Deliv. 2014, 865732.
106. Lane, H. A.; Wood, J. M.; McSheehy, P. M.; Allegrini, P. R.; Boulay, A.; Brueggen, J.; Littlewood-Evans, A.; Maira, S. M.; Martiny-Baron, G.; Schnell, C. R.; Sini, P.; O'Reilly, T. mTOR Inhibitor RAD001 (everolimus) has antiangiogenic/vascular

properties distinct from a VEGFR tyrosine kinase inhibitor. Clin. Cancer Res. 2009, 15, 5.

107. Meng, L. H.; Zheng, X. S. Toward rapamycin analog (rapalog)-based precision cancer therapy. Acta Pharmacol. Sin. 2015, 36, 1163-1169.
108. Houghton, P. J. Everolimus. Clin. Cancer Res. 2010, 16, 5, 1368-1372.
109. Faes, S.; Santoro, T.; Demartines, N.; Dormond, O. Evolving significance and future relevance of anti-angiogenic activity of mTOR inhibitors in cancer therapy. Cancers. 2017, 9, 152.
110. Albini, A.; Tosetti, F.; Li, V. W.; Noonan, D. M.; Li, W. W. Cancer prevention by targeting angiogenesis. Nat. Rev. Clin. Oncol. 2012, 1-12.
111. Damiano, V.; Rosa, R.; Formisano, L.; Nappi, L.; Gelardi, T.; Marciano, R.; Cozzolino, I.; Troncone, G.; Agrawal, S.; Veneziani, B. M.; De Placido, S.; Bianco, R.; Tortora, G. Toll-like receptor 9 agonist IMO cooperates with everolimus in renal cell carcinoma by interfering with tumour growth and angiogenesis. Br. J. Cancer, 2013, 108, 1616-1623.
112. Pignochino, Y.; Dell'Aglio, C.; Basiricò, M.; Capozzi, F.; Soster, M.; Marchiò, S.; Bruno, S.; Gammaitoni, L.; Sangiolo, D.; Torchiaro, E.; D'Ambrosio, L.; Fagioli, F.; Ferrari, S.; Alberghini, M.; Picci, P.; Aglietta, M.; Grignani, G. The Combination of Sorafenib and Everolimus Abrogates mTORC1 and mTORC2 upregulation in osteosarcoma preclinical models. Clin. Cancer Res. 2013, 19, 8, 2117-2131.
113. Iwase, Y.; Maitani, Y. Preparation and in vivo evaluation of liposomal everolimus for lung carcinoma and thyroid carcinoma. Biol. Pharm. Bull. 2012, 35, 6, 975-979.
114. Kasper, M.; Gabriel, D.; Möller, M.; Bauer, D.; Wildschütz, L.; Courthion, H.; Böhm, M. R. R.; Busch, M.; Loser, K.; Thanos, S.; Gurny, R.; Heiligenhaus, A. Novel everolimus-loaded nanocarriers for topical treatment of murine experimental autoimmune uveoretinitis (EAU). Exp. Eye Res. 2018, 168, 49-56.
115. Mishra, G. P.; Doddapaneni, B. S.; Nguyen, D.; Alani, A. W. Antiangiogenic effect of docetaxel and everolimus as individual and dual-drug-loaded micellar nanocarriers. Pharm. Res. 2014, 3, 660-669.
116. Pezeshkian, B.; Donnelly, C.; Tamburo, K.; Geddes, T.; Madlambayan, G. J. Leukemia Mediated Endothelial Cell Activation Modulates Leukemia Cell Susceptibility to Chemotherapy through a Positive Feedback Loop Mechanism. PLoS ONE. 2013, 8, 4, e60823.

117. Eichbaum, C.; Meyer, A. S.; Bischofs, E.; Steinborn, A.; Bruckner, T.; Brodt, P.; Sohn, C.; Eichbaum, M. H. R. Breast cancer cell-derived cytokines, macrophages and cell adhesion: Implications for metastasis. Anticancer Res. 2011, 31, 3219-3228.
118. Narita, T.; Kimura, N. K.; Kasai, Y.; Hosono, J.; Nakashio, T.; Matsuura, N.; Sato, M.; Kannagi, R. Induction of E-selectin expression on vascular endothelium by digestive system cancer cells. J. Gastroenterol. 1996, 31, 299-301.
119. Bischofs, E.; Lubs, D.; Fritzsche, F.; Meyer, A. S.; Bruckner, T.; Sohn, C.; Eichbaum, M. H. R. In vitro blockade of adhesion of breast cancer cells to endothelial cells using anti-inflammatory drugs. Anticancer Res. 2012, 32, 3, 767-771.
120. Bachtarzi, H.; Stevenson, M.; Šubr, V.; Ulbrich, K.; Seymour, L. W.; Fisher, K.D. Targeting adenovirus gene delivery to activated tumour-associated vasculature via endothelial selectins. J. Control. Rel. 2011, 150, 196-203.
121. Miao, Z. L.; Deng, Y. J.; Du, H. Y.; Suo, X. B.; Wang, X. Y.; Wang, X.; Wang, L.; Cui, L.J.; Duan, N. Preparation of a liposomal delivery system and its in vitro release of rapamycin. Exp. Ther. Med. 2015, 9, 3, 941-946.
122. Alba, M. A. L.; Guajardo, M. B. G.; Fonzar, J. F.; Brooks, D.E.; Sánchez, G. A. G.; Bernad, M. J. B. Preformulation studies of a liposomal formulation containing sirolimus for the treatment of dry eye disease. J. Ocul. Pharmacol. Ther. 2016, 32, 1, 11-22.
123. Gholizadeh, S.; Visweswaran, G. R. R.; Storm, G.; Hennink, W. E.; Kamps, J. A. A. M.; Kok, R. J. E-selectin targeted immunoliposomes for rapamycin delivery to activated endothelial cells. Inter. J. Phar. 2018, 548, 759-770.
124. Albini, A.; Benelli, R.; Noonan, D. M.; Brigati, C. The "chemoinvasion assay": a tool to study tumor and endothelial cell invasion of basement membranes. Int. J. Dev. Biol. 2004, 58, 563-571.
125. Tahergorabi, Z.; Khazaei, M. A review on angiogenesis and its assays. Iran J. Basic Med. Sci. 2012, 15, 6, 1110-1126.
126. Matsuki, M.; Adachi, Y.; Ozawa, Y.; Kimura, T.; Hoshi, T.; Okamoto, K.; Tohyama, O.; Mitsuhashi, K.; Yamaguchi, A.; Matsui, J.; Funahashi, Y. Targeting of tumor growth and angiogenesis underlies the enhanced antitumor activity of lenvatinib in combination with everolimus. Cancer Sci. 2017, 108, 4, 763-771.
127. Kraiss, L. W.; Weyrich, A. S.; Alto, N.M.; Dixon, D.A.; Ennis, T.M.; Modur, V.; McIntyre, T.M.; Prescott, S.M.; Zimmerman, G.A. Fluid flow activates a regulator

of translation, p70/p85 S6 kinase, in human endothelial cells. Am. J. Physiol. Heart Circ. Physiol. 2000, 278, 1537-1544.

128. Lee, D. F.; Kuo, H. P.; Chen, C. T.; Hsu, J. M.; Chou, C. K.; Wei, Y.; Sun, H. L.; Li, L. Y.; Ping, B.; Huang, W. C.; He, X.; Hung, J. Y.; Lai, C. C.; Ding, Q.; Su, J. L.; Yang, J. Y.; Sahin, A. A.; Hortobagyi, G.N.; Tsai, F.J.; Tsai, C.H.; Hung, M. C. IKKb suppression of TSC1 links inflammation and tumor angiogenesis via the mTOR pathway. Cell. 2007, 130, 440-455.

129. Zhang, J.; Gao, Z.; Yin, J.; Quon, M. J.; Ye, J. S6K directly phosphorylates IRS-1 on Ser-270 to promote insulin resistance in response to TNF-α signaling through IKK2. J. Biol. Chem. 2008, 283, 35375-35382.

130. Magnuson, B.; Ekim, B.; Fingar, D. C. Regulation and function of ribosomal protein S6 kinase (S6K) within mTOR signalling networks. Biochemical J. 2012, 441, 1-21.

131. Pende, M.; Um, S. H.; Mieulet, V.; Sticker, M.; Goss, V. L.; Mestan, J.; Mueller, M.; Fumagalli, S.; Kozma, S. C.; Thomas, G. S6K1-/- /S6K2-/- mice exhibit perinatal lethality and rapamycin-sensitive 5-terminal oligopyrimidine mRNA translation and reveal a mitogen-activated protein kinase-dependent S6 kinase pathway. Mol. Cell. Biol. 2004, 24, 8, 3112-3124.

132. Stahn, S.; Grittner, C.; Zeisig, R.; Karsten, U.; Felix, S. B.; Wenzel, K. Sialyl Lewisx-liposomes as vehicles for site-directed, E-selectin-mediated drug transfer into activated endothelial cells. Cell. Mol. Life Sci. 2001, 58, 141-147.